PHYS 6751 Laboratory: *Foil Thickness Measurements via α-Spectroscopy*

Lab overview:

- *Objective:* Measure the thicknesses of provided foils by comparing the measured energy-loss of α-particles from a provided α-source to calculations with the software SRIM and/or LISE++
- *Gain familiarity with:* α calibration sources, silicon detectors, simple vacuum systems, Monte Carlo calculations of ion interactions with matter
- *Report style:* Nuclear Instruments and Methods in Physics Research A (NIMA)

Brief description:

α-spectroscopy is a vital tool of low-energy nuclear physics, often used for nuclear structure and nuclear astrophysics studies. Silicon detectors are generally employed to determine the energy of α-particles emitted from an α-decaying source or nuclear reaction. This technique allows nuclear energy levels to be identified to either quantify the composition of an unknown radioactive sample or to identify new nuclear levels for the decay daughter of a known sample. Aside from α-energies, relative intensities for α-decay branches provide valuable additional information.

In this experiment, we will employ a radioactive calibration source of ^{226}Ra to energy-calibrate a silicon detector and to determine the thickness of aluminum and vanadium foils. Given the finite range of α-particles in air, we will employ a small vacuum chamber to perform our measurements. The source will be mounted inside of the chamber, the chamber will be evacuated ('pumped-down'), and a spectrum will be taken to perform the energy calibration. Two foils will separately be inserted in between the source and the detector and the thickness of each foil will be determined by comparing the energy loss to calculated and/or tabulated values. Additional tasks include determining the age of the ^{226}Ra source, it's activity, and the number of ^{226}Ra atoms remaining in the source.

Expectations for Run-plan:

The run-plan should consist of time-saving calculations and an order of operations. For instance,

- What are expected α–energies for ^{226}Ra and its decay products?
- How is the source age calculated from the relative intensity of ^{226}Ra and its decay products?
- What is the experiment order-of-operations? (e.g. When do we bias?, What is the bias voltage to apply?, When do we pump-down?, When to we mount foils?, etc.)
- How will the data analysis be performed? (e.g. peak-fitting, background subtraction)
- How can we determine the α–detection efficiency?

- What is the maximum thickness we can measure for our foils with our source?
- Sample calculations for energy-loss compared to data tables and/or other calculations (e.g. SRIM vs LISE++ Physical Calculator vs data table)
- Do the foils impact the detection efficiency?
- ...of course, other preparatory notes are welcome, so long as they're useful!

NOTE: The above examples are suggestions. Please do not feel obligated to have all of them done prior to the lab start. You will be working in a group, so with any luck your partners will have prepared for some different portions of the lab.

Expectations for Lab Report:

The lab report should be a publication-quality paper typeset in the style of Nuclear Instruments and Methods in Physics Research Section A. As such, it should include a brief motivation for our measurement, a technical description of the set-up, and a thorough description of the experimental methods, along with benchmarking against simulations.

The reports will be written individually, but your group members should appear as co-authors on the paper. As such, you are free to share calculations and plots. In fact, sharing in this sense is expected, as this is how real experiments work. However, all writing must be your own.

NOTE: It is quite possible that the lab contains more work than you could possibly get done during the experiment time allotted. This is OK, as I don't expect you to necessarily complete every single task. However, a reasonable amount of work must be completed and that work must be thoroughly described in an articulate way.

WARNINGS:

- Be careful with the bias voltage
  - Don't electrocute yourself
  - Don't exceed the maximum bias voltage for the detector
  - Don't apply voltage when vacuum is bad
  - Don't apply voltage to a detector exposed to light
- Be careful with the α-source
  - Only handle with gloves
  - Never touch the surface of the α-source to any other surface
  - Report any incidents (e.g. dropped the source) immediately to Zach Meisel or Tom Massey or Carl Brune
- Be careful when venting
  - Don't accidentally evacuate oil into the chamber
- If you aren't sure, ask!

Appendices

1. Electronics set-up
2. Ortec α-spectrocsopy information
3. ^{226}Ra α-decay chain
4. ^{226}Ra decay-chain information
5. ^{226}Ra example spectrum
6. Notes on ^{226}Ra age determination
7. ^{226}Ra source specifications
8. Si-detector specifications
9. Comments on radioactive decay
10. Comments on α-decay
11. Ortec α energy-loss information
12. Plots of α ranges and energy loss
13. SRIM introduction
14. LISE++ introduction & physical calculator
15. Comments on energy loss of ions in matter

C. Brune

Electronics Setup

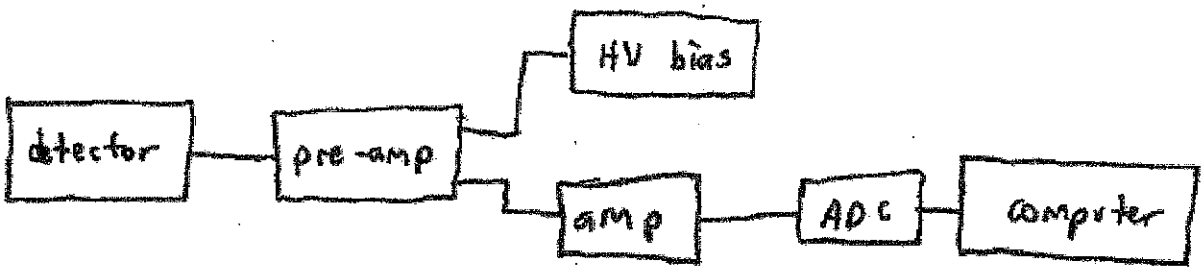

- The chamber must be evacuated before starting the measurements. Do not leave the high-voltage bias on when either pumping out or venting the chamber. Any ideas why?
- The bias voltage for our detector BA-024-300-500 is 250 V.
- The detector is connected to a pre-amplifier by a single coaxial cable.
- The high-voltage bias for the detector is supplied to the preamp.
- The pre-amp output is sent to an amplifier.
- The amplifier output is sent to an ADC.
- The digital data from the ADC is stored in the computer.

ORTEC®

Experiment 4
Alpha Spectroscopy with Silicon Charged-Particle Detectors

Equipment Required

- ULTRA™ Charged Particle Detector model **BU-014-050-100**
- **142A** Preamplifier
- **4001A/4002D** NIM Bin and Power Supply
- **575A** Spectroscopy Amplifier
- **807** Vacuum Chamber
- **428** Detector Bias Supply
- **480** Pulser
- **EASY-MCA-8K** including a USB cable and MAESTRO software (other ORTEC MCAs may be substituted)
- **C-36-12** RG-59A/U 75 Ω Coaxial Cable with SHV Plugs, 12-ft (3.7-m) length.
- **C-24-1/2** RG-62A/U 93 Ω Coaxial Cable with BNC Plugs, 0.5-ft. (15-cm) length.
- Two **C-24-4** RG-62A/U 93 Ω Coaxial Cables with BNC Plugs, 4-ft. (1.2-cm) length.
- Two **C-24-12** RG-62A/U 93 Ω Coaxial Cables with BNC Plugs, 12-ft (3.7-m) length.
- **C-29** BNC Tee Connector
- **ALPHA-PPS-115** Portable Vacuum Pump Station
- Personal Computer with a USB port and a recent, supportable version of the Windows operating system.
- Access to a suitable printer for printing/plotting spectra acquired with MAESTRO.
- **TDS3032C** Oscilloscope with a bandwidth ≥150 MHz.
- **AF200*** Alpha Source Set including 0.1 μCi of ^{241}Am, 0.01 μCi of ^{228}Th and 0.01 μCi of ^{230}Th.
- **AF-244-A2-0.1*** Alpha Source consisting of 0.1 μCi of ^{244}Cm.
- Small, flat-blade screwdriver for tuning screwdriver-adjustable controls.

*Sources are available direct from supplier. See the ORTEC website at www.ortec-online.com/Service-Support/Library/Experiments-Radioactive-Source-Suppliers.aspx

Purpose

The purpose of this experiment is to familiarize the student with the use of silicon charged-particle detectors and to study some of the properties of alpha-emitting isotopes. It should take about 6 hours to complete all parts of Experiment 4. The parts are written so that they can be completed in two 3-hour laboratory periods, or certain parts can be easily omitted if equipment time is not available.

Silicon Charged-Particle Detectors

Semiconductor charged-particle detectors have been used extensively in experimental nuclear research since the early 1960s, when they revolutionized nuclear particle detection. The development rode the coattails of the emerging silicon wafer technology used in making silicon transistors. Compared to the previously employed scintillation detectors, gas proportional counters or ionization chambers, the silicon charged-particle detector offers significantly better energy resolution, excellent long-term gain stability, and much more compact size. Following the successful development of the silicon semiconductor charged-particle detector, the more difficult development of Germanium semiconductor detectors for gamma-ray spectrometry ensued. Concurrently, Si(Li) semiconductor detectors for X-ray spectrometry were also developed. Semiconductor detectors became popular because of their superior energy resolution. The better energy resolution derives from the higher number of electron-hole pairs created in silicon for a particle of energy E compared to the lower number of electron-ion pairs created in a gas proportional counter. Thus, the percent statistical fluctuation in the amount of charge collected with the semiconductor detector is smaller, and this means better energy resolution.

The semiconductor detectors for photon spectrometry will be studied in a later experiment. This experiment concentrates on the silicon semiconductor detector and its application to alpha-particle spectrometry.

Semiconductor charged-particle detectors can be used through an extensive range of energies, including 20 keV electrons on one end of the spectrum and 200 MeV heavy ions on the other. The inherent resolution of ion-implanted and surface barrier detectors is surpassed only by magnetic spectrometers. The detector output pulses rise rapidly. Hence, they are well suited for fast (~1 ns) timing with coincidence circuitry or time-to-amplitude converters (TACs).

The efficiency of silicon charged-particle detectors for their active volume is essentially 100%, and their energy versus pulse-height curves are linear over a rather impressive range. The remaining fact of particular interest in the educational market is that they are relatively inexpensive.

Experiment 4
Alpha Spectroscopy with Silicon Charged-Particle Detectors

Detector Operating Principles

Basically, the silicon charged-particle detector is a rather large semiconductor diode with a very thin window to allow the charged particles to enter at the front surface with minimal energy loss. By applying a reverse bias to the diode, virtually all of the free charge carriers are swept out of the sensitive depth of the diode. The depth of this charge-free zone is known as the depletion depth. The data sheet supplied with the detector will specify the reverse bias voltage required to achieve the desired depletion depth. Operating at a lower bias voltage will reduce the depletion depth. Because the front and rear electrodes form a parallel-disc capacitor, the detector capacitance is inversely proportional to the depletion depth. To achieve the best signal-to-noise ratio and good energy resolution, it is important to minimize the detector capacitance and any other stray capacitance hanging on the preamplifier input. See the ORTEC 142A/B/C Preamplifier data sheet for more information (ref. 9).

When a charged particle, such as an alpha particle, enters the detector, it loses a small amount of energy in the thin entrance window. The vast majority of its energy is deposited in the depleted region of the detector diode by causing ionization of the silicon atoms. The number of electron-hole pairs created in the silicon diode by this process is proportional to the energy of the incident alpha particle. This free charge, created by the ionization, is swept to the electrodes where it is collected on a small feedback capacitor by the preamplifier. The result at the output of the preamplifier is a pulse that rises within 1 to 100 ns to a voltage determined by the collected charge and the size of the feedback capacitor. The amplitude of this voltage step is proportional to the energy of the detected alpha particle.

To make room for successive events, the preamplifier output signal decays back to zero volts with a 50-μs exponential decay time constant. The amplifier processes this signal by applying low-pass and high-pass filters to improve the signal-to-noise ratio and to further limit the duration of each pulse. It also applies an adjustable gain to boost the pulse heights into the range required by the Multichannel Pulse-Height Analyzer. At the output of the amplifier, the pulse height is still proportional to the energy of the detected alpha particle. The task of the Multichannel Analyzer is to sort these pulse heights into a histogram that represents the energy spectrum of the alpha particles.

For further information on the Multichannel Pulse-Height Analyzer, see the description in the Educational Experiments Library (www.ortec-online.com/Solutions/educational.aspx).

Types of Silicon Charged-Particle Detectors

The original silicon semiconductor detector used a surface-barrier contact to form the diode junction on the front surface of the detector. Essentially, this is a wisp of gold evaporated over a thin silicon oxide layer on the surface of the silicon wafer. This contact is very fragile, and one must avoid touching it. A fingerprint on the gold surface is enough to destroy the diode characteristics of the detector. Once ion-implantation technology was developed, a more rugged front contact was formed by implanting boron atoms to a controlled depth in the silicon wafer. A similar ion-implantation process with a different ion is used to form the rear contact. Although the ion-implanted window can be cleaned with alcohol on a clean, soft, cotton swab, one must avoid scratching the front surface with abrasive dust particles. The front contact is about 500 Ångstroms thick, and a small scratch can render this contact dysfunctional.

Ion-implanted detectors benefit from an order of magnitude lower leakage current, and this means lower electronic noise at longer amplifier shaping time constants. Surface-barrier detectors usually operate with a 0.5 μs shaping time constant, whereas ion-implanted silicon detectors typically employ a 1 μs amplifier shaping time constant.

Critical Detector Parameters

There are three main parameters that define silicon charged-particle detectors: energy resolution, active area, and depletion depth. ORTEC model numbers reflect each of these three parameters in that order. The BU-014-050-100 listed for this experiment is an ULTRA™ (ion-implanted) detector with an energy resolution <14 keV FWHM for ^{241}Am alphas, an active area of 50 mm^2, and a minimum depletion depth of 100 μm. The letter "B" in the model number designates a Microdot connector centered on the rear of the detector, and the "U" specifies the ULTRA ion-implanted detector structure. The quoted energy resolution of an ORTEC detector is a measure of its quality. These resolutions can be measured only with a complete set of electronics, calibrated for standard conditions. The ORTEC guaranteed resolutions are measured with standard ORTEC electronics. A resolution of 20 keV or better is satisfactory for all parts of Experiment 4.

For semiconductor photon detectors, relatively simple mathematical models describe the energy resolution as a function of energy. But, charged-particle spectroscopy with silicon semiconductor detectors involves so many complicated processes, that it is not possible to describe the energy resolution versus energy with a simple mathematical model. See ref. 1, Chapters 2 and 11 for details. However, there are principles for obtaining optimum energy resolution. These involve:

- Minimizing materials that can cause varying energy losses for the alpha particles as they travel to the detector.
- Minimizing the range of incidence angles with which the alpha particles impinge on the detector.
- Choosing a detector with minimum dead layer thickness and low leakage current.
- Using the optimum shaping time constant on the amplifier.
- Avoiding contamination of the detector window.
- Preventing damage to the detector front contact.

Since the shape of the detector is a circular disk, its active area is determined by the diameter of its face. At any given distance from the source, a larger area will subtend a larger angle, and thus intercept a greater portion of the total number of alpha particles that emanate from the source. A nominal area of 50 mm^2 is suggested for this experiment. But, any area from 25 through 100 mm^2 will provide the information.

The depletion depth is synonymous with the sensitive depth of the detector. For any experiment, the depth must be sufficient to completely stop all the charged particles that are to be measured. The ability to meet that requirement is dependent upon both the energy and the particle type. Fig. 4.1 is a range-energy curve for five of the more common charged particles. From that graph, the minimum depth for the maximum energy of a particle type can be determined. From Fig. 4.1, note that a 5.5 MeV alpha is completely stopped by ~27 μm of silicon. Since natural alphas are usually <8 MeV in energy, a detector with a 50 μm depletion depth is adequate to stop all natural alphas.

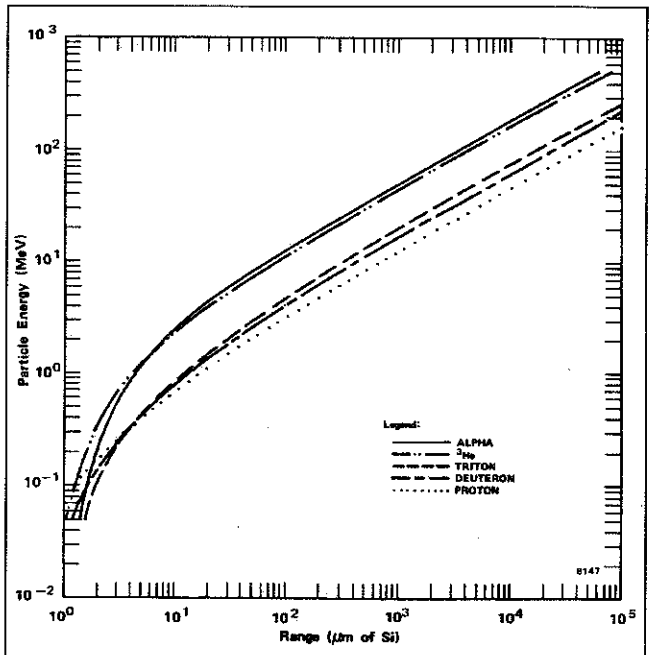

Fig. 4.1. Range-Energy Curves for Charged Particles in Silicon. [Data taken from ref.10.]

For an ion-implanted silicon detector, the Boron-implanted front contact causes a dead layer of approximately 500 Ångstroms thickness. Any ionization caused by the alpha particle, as it loses energy in this dead layer, recombines before it can be collected. Thus, there will be a deficit in the measured energy of the alpha particle equal to the energy the particle loses in the dead layer at the entrance window.

Fig. 4.2 illustrates the stopping power for various types of charged particles in Silicon and Germanium detectors. The stopping power in the graph is actually $(1/\rho)(dE/dx)$, where ρ is the density of silicon (2.33 g/cm^3), and dE is the incremental energy lost over the incremental distance dx. For example, a 5 MeV alpha particle will lose approximately 7 keV of energy in the 500 Å dead layer of an ULTRA ion-implanted silicon detector. Note that the rate of energy loss varies with the initial energy of the alpha-particle. See ref. 1–4, 7 and 8.

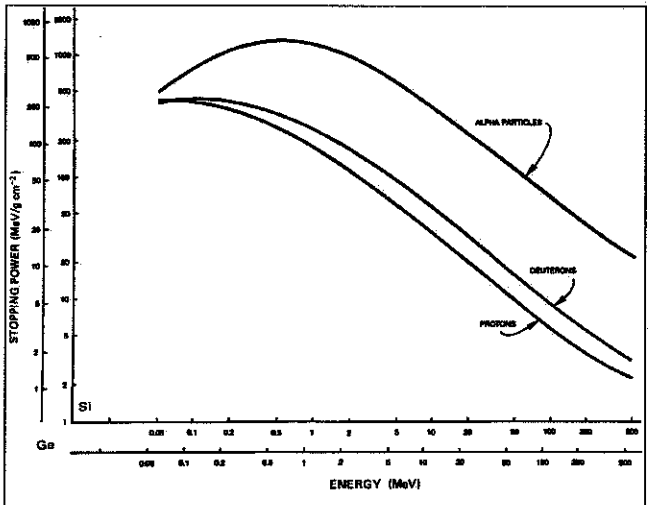

Fig. 4.2. Stopping power vs. Energy for Protons, Deuterons, and Alpha Particles in Si and Ge.

Detector Leakage Current Issues

One of the reasons for choosing an ion-implanted silicon detector instead of a surface-barrier detector is the much lower leakage current of the former compared to the latter. With a surface-barrier detector, one must always compensate for the voltage drop caused by the leakage current when setting the bias voltage. There is a 100 MΩ resistor between the BIAS input and the detector INPUT connector on the 142A Preamplifier. The function of that resistance is to suppress high-frequency noise from the bias supply, and allow virtually all of the charge from the detector to reach the preamplifier input.

Surface-barrier detectors have a typical leakage current of the order of 50 nA. Such a high leakage current would cause a 5 V drop in voltage across the 100 MΩ resistor. Therefore, one would have to raise the voltage of the detector bias supply by 5 V above the desired bias voltage to achieve the specified bias voltage at the detector. This can be a significant adjustment when the bias voltage for the detector is normally in the range of 50 to 100 V.

Experiment 4
Alpha Spectroscopy with Silicon Charged-Particle Detectors

For ion-implanted silicon detectors, leakage currents are normally of the order of 1 nA at room temperature. That leakage current will increase by about a factor of 2 for every 7°C increase in temperature. Such low leakage currents generate a voltage drop of the order of 0.1 V across the 100 MΩ detector bias resistor. Thus, there is no need to compensate for the voltage drop with ion-implanted silicon detectors.

Alpha Sources

CAUTION: Alpha sources offer a potential contamination problem. Never touch the face of a source with your fingers. Most alpha sources are electrodeposited onto platinum disks. The actual radioactive source is usually a spot ~1 mm diameter deposited in the geometrical center of the disk. If you look carefully, you may be able to see the deposited spot. ALWAYS handle an alpha source by the edge of the mounting disk.

Because alpha-particles lose energy easily in thin layers of material, the deposited radioactive material must be very thin, and the sources must have either no window or an extremely thin window over the deposited radioactive material. Any significant energy loss in the radioactive material or the window will reduce the measured energy of the alpha particle, and variations in that energy loss will broaden the energy resolution in the acquired spectrum. Dirt or other contamination that collects on the surface of the source can also contribute to undesirable energy loss and resolution broadening. Therefore the source should always be stored in a protective container when not in use. The absence of a protective window over the source means that there is potential for the radioactive material to be knocked loose from the source substrate and to disperse into surrounding areas. Some naturally-occurring alpha-emitters decay into a radioactive daughter isotope that is a gas (Radon). This gas can leave the source and cause contamination of the surrounding environment with its radioactive daughter isotopes.

Because of the issues with migration of the radioactive source material and dirt deposits on the surface of the source, alpha-source manufacturers generally recommend replacing the alpha source every two years.

For further advice on alpha sources consult ref. 10.

EXPERIMENT 4.1. Simple Alpha Spectrum and Energy Calibration with a Pulser

Procedure

Connecting the Electronic Instruments.

1. Set up the equipment as shown in Fig. 4.3, with the 807 Vacuum Chamber connected to the ALPHA-PPS-115 Portable Vacuum Pump Station via the vacuum hose.
2. Check that the ULTRA Charged Particle Detector model BU-014-050-100 has been properly installed in the vacuum chamber lid.
3. To minimize the stray capacitance on the preamplifier input, connect the detector output to the 142A Preamplifier INPUT using the shortest possible 93 Ω coaxial cable (C-24-1/2).

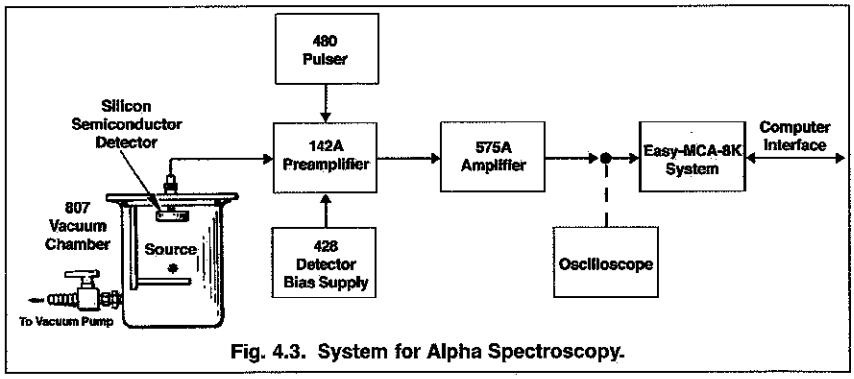

Fig. 4.3. System for Alpha Spectroscopy.

4. Check that the SHAPING TIME switches accessible through the side panel of the 575A Amplifier are all set to 1.5 μs.
5. Turn off power to the 4001A/4002D NIM Bin and Power Supply, and insert the 480 Pulser, 428 Detector Bias Supply, and 575A Amplifier in the NIM Bin.
6. Connect the captive power cable on the 142A Preamplifier to the PREAMP POWER connector on the rear panel of the 575A Amplifier.
7. Using a 3.7 m, 93 Ω, coaxial cable, connect the Preamplifier "E" (Energy) output to the INPUT of the 575A Amplifier. Set the 575A input polarity to POSitive.
8. On the 428 Detector Bias Supply, set both voltage dials to their minimum value (zero). Turn the POS/OFF/NEG switch to the OFF position.

Tosaka

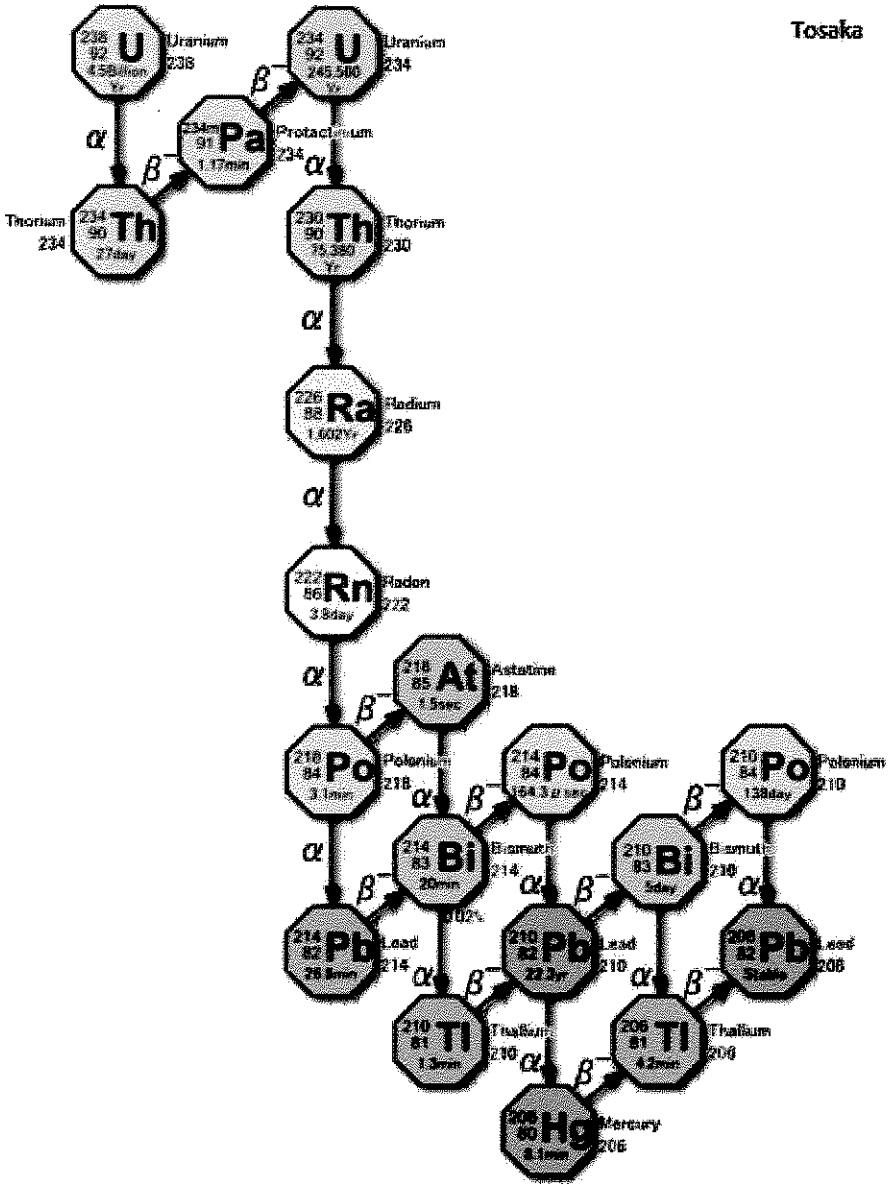
U
Uranium
238
Pa
Protactinium
234
U
Uranium
234
Th
Thorium
234
Th
Thorium
230
Ra
Radium
226
Rn
Radon
222
At
Astatine
218
Po
Polonium
218
Po
Polonium
214
Po
Polonium
210
Bi
Bismuth
214
Bi
Bismuth
210
Pb
Lead
214
Pb
Lead
210
Pb
Lead
206
Tl
Thallium
210
Tl
Thallium
206
Hg
Mercury
206

C. Brune

Appendix 1: Decay of ^{226}Ra

88-Ra-226 Radium-226
Half-life: 1600 years
Mode of decay: alpha into Rn-222
Decay energy: 4.871 MeV
Subsequently γ radiation of Rn-222 at 186 keV possible

86-Rn-222 Radon-222, noble gas
Half-life: 3.8235 days
Mode of decay: alpha into Po-218
Decay energy: 5.590 MeV

84-Po-218 Polonium-218 (Historically Po-218 is also called radium A)
Half-life: 3.10 minutes
Mode of decay: alpha into Pb-214
Probability: 99.98 %
Decay energy: 6.115 MeV
Mode of decay: beta into At-218
Probability: 0.02 %
Decay energy: 0.265 MeV

85-At-218 Astatine-218
Half-life: 1.5 seconds
Mode of decay: alpha into Bi-214
Probability: 99.90 %
Decay energy: 6.874 MeV
Mode of decay: beta into Rn-218
Probability: 0.1 %
Decay energy: 2.883 MeV

86-Rn-218 Radon-218
Half-life: 35 milliseconds
Mode of decay: alpha into Po-214
Decay energy: 7.263 MeV

82-Pb-214 Lead-214 (Historically Pb-214 is also called radium B)
Half-life: 26.8 minutes
Mode of decay: beta into Bi-214
Decay energy: 1.024 MeV
Subsequently γ radiation of Bi-214 at 352 keV, 295 keV, 242 keV, 53 keV possible

83-Bi-214 Bismuth-214 (Historically Bi-214 is also called radium C)
Half-life: 19.9 minutes
Mode of decay: beta into Po-214
Probability: 99.98 %

C. Bare

Decay energy: 3.272 MeV
Subsequently γ radiation of Po-214 at 609 keV possible
Mode of decay: alpha into Tl-210
Probability: 0.02 %
Decay energy: 5.617 MeV

84-Po-214 Polonium-214 (Historically Po-214 is also called radium C')
Half-life: 164.3 ms
Mode of decay: alpha into Pb-210
Decay energy: 7.833 MeV

81-Tl-210 Thallium-210 (Historically Tl-210 is also called radium C")
Half-life: 1.3 Minutes
Mode of decay: beta into Pb-210
Decay energy: 5.484 MeV

82-Pb-210 Lead-210 (Historically Pb-210 is also called radium D)
Half-life: 22.3 years
Mode of decay: beta into Bi-210
Decay energy: 0.064 MeV
Mode of decay: alpha into Hg-206
Probability: 1.9E-6 %
Decay energy: 3.792 MeV

83-Bi-210 Bismuth-210 (Historically Bi-210 is also called radium E)
Half-life: 5.013 days
Mode of decay: beta into Po-210
Decay energy: 1.163 MeV
Mode of decay: alpha into Tl-206
Probability: 0.00013 %
Decay energy: 5.037 MeV

84-Po-210 Polonium-210 (Historically Po-210 is also called radium F)
Half-life: 138.376 days
Mode of decay: alpha into Pb-206
Decay energy: 5.407 MeV

82-Pb-206 Lead-206 (Historically Pb-206 is also called Radium G)
Pb-206 is the final product of the U-238 radioactive series. It is stable. This lead is dead!

The entries are taken from the NUDAT database, see:

R.R.Kinsey, et al.,The NUDAT/PCNUDAT Program for Nuclear Data, paper submitted to the 9th International Symposium of Capture Gamma-ray Spectroscopy and Related Topics, Budapest, Hungary, October 1996. Data extracted from NUDAT database (Dec.18, 1997).

S. Chałupnik et al. Adv. Lq. Scint. Spectrom. 2007

t-counting time (min); A-activity of the ^{226}Ra standard (Bq); N-number of counts for the standard sample.

From our measurements we obtained the following values: N_p = 22 counts; N = 1757 counts; t = 1440 (min); A = 2.22 (Bq); V = 0.05 (L). So, the calibration factor was calculated as k ≈ 5 (cpm/Bq). Therefore, the limit of detection equals LLD = 0.04 (Bq/L)].

Calibration of the Spectrometer

We bought the radium standard ^{226}Ra from Amersham. From that standard we made a standard solution with the activity 222.0 Bq/L ^{226}Ra. For the preparation of the standard sample 10 mL of standard solution was used, so it is equal 2.22 Bq ^{226}Ra per sample. The calibration factor was calculated on the basis of several replicate measurements of standard samples. The value of that factor for our spectrometer is of about 5 (cpm/Bq).

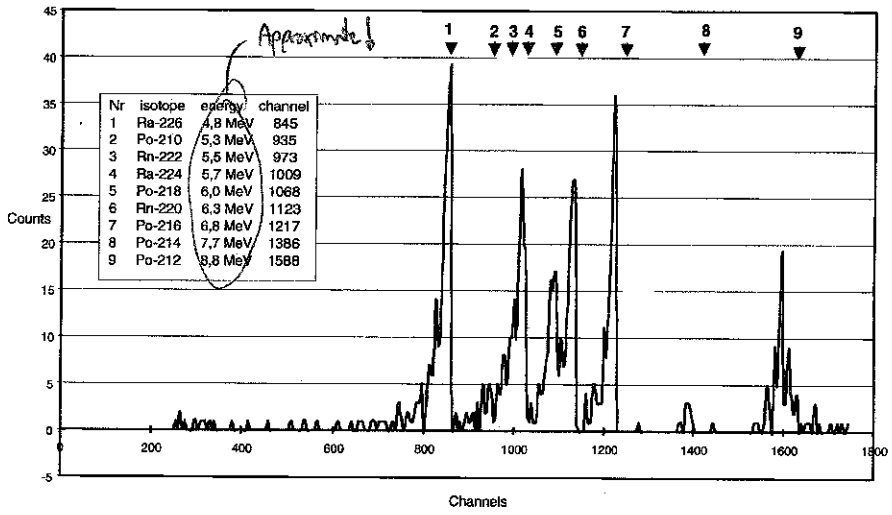

Figure 2 Alpha spectrum of the reference sample

Reference Samples

Mine water was used as the reference sample. This water has been sampled from a Polish coal mine. It is brine, containing radium and sulphate ions, but no barium (so called water type B). This particular water is also a reference sample in the liquid scintillation laboratory, measured several times per month. Therefore, the concentration of radium isotopes in this sample is very well known. The activity of ^{226}Ra in reference sample is equal in average 1.86 ± 0.15 kBq/m^3. The alpha spectrum obtained for the reference sample is shown in Figure 2.

The reference sample was prepared several times and measured as replicate samples to check the accuracy of the method. The activity of ^{226}Ra in the reference, calculated on the basis of results from alpha spectrometry, equals 1.78 ± 0.18 kBq/m^3. So, good agreement of both methods was reached.

APPLICATION OF THE METHOD

At first, we planned to use the alpha spectrometric method of radium analysis (^{226}Ra) for monitoring of the radium removal process. But the method was tested during our survey of radium content in

C. Bruce

Physics 373
May 2005 / May 2007

Some Remarks on Determining the "age" of a ^{226}Ra Source

Assuming that one starts with pure ^{226}Ra, it is possible to determine its "age" (defined here to be the time since it started life in a pure state) by observing the decays of its daughter products. First note that all the decay half-lives are very short (less than one week), except for two: the initial ^{226}Ra decay ($t_{1/2} = 1600$ years) and the the ^{210}Pb decay ($t_{1/2} = 22.3$ years).

The number of ^{226}Ra atoms N_A present in the source is a function of time t and is described by

$$N_A = N_0 \exp(-t/\tau_A), \tag{1}$$

where $N_0 = N_A(0)$ and τ_A is the mean lifetime of ^{226}Ra given by $t_{1/2}/\ln 2$. The decay rate of ^{226}Ra is given by

$$-\frac{dN_A}{dt} = N_A/\tau_A. \tag{2}$$

I will assume $t = 0$ when the source was made. Note that $\frac{dN_A}{dt}$ is a quantity that you can measure in the laboratory and can be used to determine N_A.

Once the source is several weeks old, an equilibrium is established. Consider for example ^{222}Rn. In equilibrium, this isotope is produced at essentially the same rate as which is it decays – this must be the case because every ^{222}Rn which is created decays shortly thereafter. This same argument can be applied to all of the other isotopes in the decay chain which have short half-lives (i.e. less than one week). Unfortunately, these decays don't tell us anything about the age of the source.

For ^{210}Pb and ^{206}Pb we have to be a little bit more careful. Once the source is several weeks old, ^{210}Pb is produced at the same rate as ^{226}Ra decays. However, ^{210}Pb decays with a 22.3-year half-life. We can describe the number of ^{210}Pb atoms N_B as a function of time via:

$$\frac{dN_B}{dt} = -\frac{dN_A}{dt} - \frac{N_B}{\tau_B} \tag{3}$$

$$= \frac{N_0}{\tau_A}\exp(-t/\tau_A) - \frac{N_B}{\tau_B}. \tag{4}$$

The first term in this equation describes the creation of N_B by the decays of parent nuclei and the second term describes the decay of N_B due to its own half-life (τ_B is the mean lifetime of ^{210}Pb).

This is a differential equation. It can be solved by "guessing" the answer:

$$N_B = A\exp(-t/\tau_A) + B\exp(-t/\tau_B), \tag{5}$$

Where A and B are arbitrary constants. If we start with a pure ^{226}Ra source that means we have zero ^{210}Pb initially so we have $N_B(t = 0) = 0$, i.e. $A = -B$. We can determine A by substituting in Eq. (4); the final result is:

$$N_B = \frac{N_0}{\tau_A/\tau_B - 1}\left[\exp(-t/\tau_A) - \exp(-t/\tau_B)\right]. \tag{6}$$

The quantity N_B *does* tell us something about the age of the source. Unfortunately neither N_B or its decay rate can be measured directly with our setup (^{210}Pb decays by β emission).

We can apply the equilibrium argument to decays following ^{210}Pb. In particular, the decay rate of ^{210}Po is equal to the decay rate of ^{210}Pb once the source is several weeks old. The nucleus ^{210}Po decays by α emission – something which we can measure. In addition the ^{210}Po decay rate is just given by $\frac{N_B}{\tau_B}$ – something we can calculate from Eq. (6)! The comparison can be used to determine t – the age of the source.

C. Brune

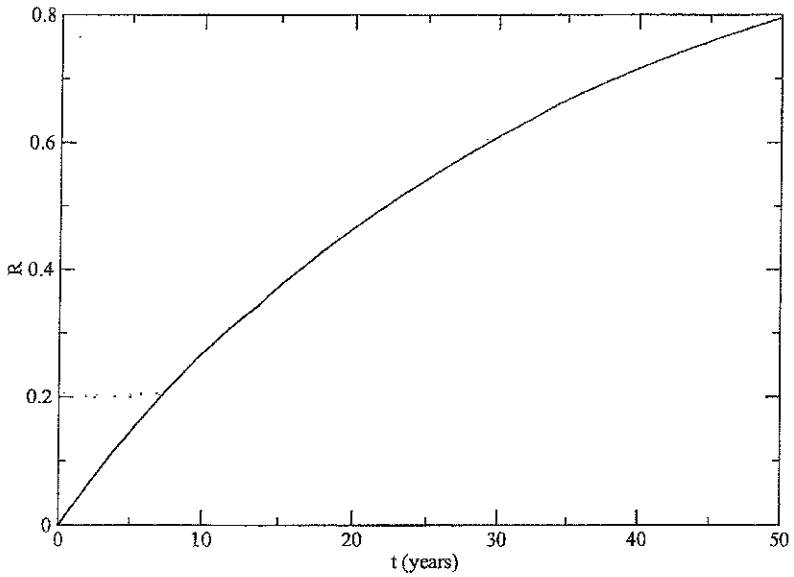

Figure 1: The ratio R as a function of the age t.

May 2007 Addenda:

Here is some more of the algebra you need to use. The decay rates of ^{226}Ra and ^{210}Pb are given by

$$\frac{N_A}{\tau_A} = \frac{N_0}{\tau_A}\exp(-t/\tau_A) \quad \text{and} \tag{7}$$

$$\frac{N_B}{\tau_B} = \frac{N_0}{\tau_A - \tau_B}\left[\exp(-t/\tau_A) - \exp(-t/\tau_B)\right]. \tag{8}$$

There is a subtle point here: the "decay rate" and and "rate of change" are not the same thing for ^{210}Pb since the rate of change also includes production. Taking the ratio, one obtains

$$R \equiv \frac{N_B\tau_A}{N_A\tau_B} = \frac{\tau_A}{\tau_A - \tau_B}\left[1 - \exp(-t/\tau_B + t/\tau_A)\right]. \tag{9}$$

The ratio R as a function of the age t is shown in Fig 1. Note also that the ratio R is also equal to the measured ratio of ^{210}Po decay αs to ^{226}Ra decay αs. Equation (9) can then be inverted to find the age t:

$$t = -\frac{\tau_A\tau_B}{\tau_A - \tau_B}\ln\left(1 - R\frac{\tau_A - \tau_B}{\tau_A}\right). \tag{10}$$

Isotope Products Laboratories
An Eckert & Ziegler Company

24937 Avenue Tibbitts
Valencia, California 91355

Tel 661•309•1010
Fax 661•257•8303

CERTIFICATE OF CALIBRATION
ALPHA STANDARD SOURCE

Radionuclide:	Ra-226	**Customer:**	OHIO UNIVERSITY---PAYABLES
Half-life:	1600 ± 7 years	**P.O. No.:**	OU 10929
Catalog No.:	AF-226-A1	**Reference Date:**	1-Sep-06 12:00 PST
Source No.:	1198-84	**Contained Radioactivity: (Ra-226 only)**	0.08827 µCi 3.266 kBq

Physical Description:

A.	Capsule type:	A-1
B.	Nature of active deposit:	Electrodeposited and diffusion bonded oxide
C.	Active diameter/volume:	5 mm
D.	Backing:	Platinum clad nickel
E.	Cover:	Approximately 50 µg Au/cm²

CAUTION!
DELICATE SURFACE
DO NOT WIPE
ACTIVE AREA

Radioimpurities:

None detected (daughters not in equilibrium)

Method of Calibration:

This source was assayed using an alpha spectrometry surface barrier detector against a standard of similar isotopic composition and geometric configuration.

Uncertainty of Measurement:

A.	Type A (random) uncertainty:	± 0.7 %
B.	Type B (systematic) uncertainty:	± 3.0 %
C.	Uncertainty in aliquot weighing:	± 0.0 %
D.	Total uncertainty at the 99% confidence level:	± 3.1 %

Notes:

- See reverse side for leak test(s) performed on this source.
- IPL participates in a NIST measurement assurance program to establish and maintain implicit traceability for a number of nuclides, based on the blind assay (and later NIST certification) of Standard Reference Materials (as in NRC Regulatory Guide 4.15).
- Nuclear data was taken from NCRP Report No. 58, 1985.
- This source has a working life of 2 years.

Daniel James Van Dalsen
Quality Control

7-Aug-06
Date

IPL Ref. No.: 1198-84

ORTEC
INCORPORATED
100 MIDLAND ROAD · OAK RIDGE · TENNESSEE 37830
AN EG&G COMPANY
TELEPHONE (615) 482-4411 TELEX 55-7450

QUALITY ASSURANCE DATA
Semiconductor Radiation Detectors

WARRANTY BASIS

Shipment Date 10-11-76 Serial No. 16-1790

Model No. BA 024-300-500

Active Area (nominal) 300 mm²

Alpha Resolution 24 Kev FWHM(a)

Noise width 19 Kev FWHM(b)

Sensitive Depth (minimum) 500 microns

Operating Bias 300 volts

Pos ☒ Neg ☐

ACTUAL MEASUREMENTS

Alpha Resolution 20.3 Kev FWHM(a)

Noise width 16.0 Kev FWHM(b)

Reverse Current 0.95 μamps @ 250 volts

Temperature 23 °C

Sensitive Thickness ≥ 500 microns

Nominal Resistivity 6500 Ωcm.

Electrode Thickness: Au 40.3 μgm/cm²

Al 40.0 μgm/cm²

NOTES:

WARRANTY TERMS

Detectors are guaranteed to meet the minimum specifications of the warranty basis data above for a period of 12mo from the date of shipment if used in careful laboratory conditions as outlined in the ORTEC Detector Instruction Manual. During the term of the original warranty period the detector will be repaired or replaced at ORTEC option, at no charge to the user with service credit extended for unused portion of warranty period from date of notification of failure.

ORTEC makes no other warranties, express or implied, and specifically NO WARRANTY OF MERCHANTIBILITY OR FITNESS FOR A PARTICULAR PURPOSE.

ORTEC's exclusive liability is limited to repairing or replacing, at ORTEC's option, items found by ORTEC to be defective in workmanship or materials within one year from the date of delivery. ORTEC's liability on any claim of any kind, including negligence, loss or damages arising out of, connected with, or from the performance or breach thereof, or from the manufacture, sale, delivery, resale, repair, or use of any item or services covered by this agreement or purchase order, shall in no case exceed the price allocable to the item or service furnished or any part thereof that gives rise to the claim. In no event shall ORTEC be liable for special or consequential damages.

GENERAL SPECIFICATIONS

1. All detectors are operated in excess of 12 hours in vacuum of 10^{-6}mm of Hg before taking data shown.

2. Surface barrier type detectors have a front surface dead layer no greater than that corresponding to 20 Kev energy loss from a 5.5 Mev alpha.

a. Alpha resolution is the full-width at half-maximum (FWHM) of a 5.5 Mev thin Am^{241} alpha source spectrum line, measured with detector and source in vacuum, with stated high voltage, and includes the noise contribution of an ORTEC Amplifier System.

b. Noise Width is the FWHM of an ORTEC precision pulse generator line spectrum with detector connected as a noise source to input of an ORTEC Amplifier System, and at stated bias voltage. Noise width is generally somewhat less than alpha resolution, and is very nearly equal to beta or proton resolution for totally absorbed particles.

Data Certified by Reba E Heath

Special Test Data

nuclear masses, nuclei can decay spontaneously into two or more lighter nuclei, provided the mass of the parent nucleus is larger than the sum of the masses of the daughter nuclei.

Most such nuclei decay via two-body decays and the commonest case is when one of the daughter nuclei is a ^{4}He nucleus (i.e. an α particle: $^4\text{He} \equiv 2p2n$, with $A = 4$, $Z = N = 2$). The α particle is favoured in such decays because it is a very stable, tightly bound structure. Because this is a two-body decay, the α particle has a unique energy and the total energy released, the *Q-value*, is given by:

$$Q_\alpha = (M_P - M_D - M_\alpha)c^2 = E_D + E_\alpha, \tag{2.60}$$

where the subscripts refer to parent and daughter nuclei and the α particle, and E is a kinetic energy.

The term *fission* is used to describe the rare cases where the two daughter nuclei have similar masses. If the decay occurs without external action, it is called *spontaneous fission* to distinguish it from *induced fission*, where some external stimulus is required to initiate the decay. Spontaneous fission only occurs with a probability greater than that for α emission for nuclei with $Z \geq 110$. The reason for this is discussed below in Section 2.7.

Nuclei may decay by the emission of photons, with energies in the gamma ray part of the electromagnetic spectrum (*gamma emission*). This occurs when an excited nuclear state decays to a lower state and is a common way whereby excited states lose energy. The lower energy state is often the ground state. A competing process is *internal conversion*, where the nucleus de-excites by ejecting an electron from a low-lying atomic orbit. Both are electromagnetic processes. Electromagnetic decays will be discussed in more detail in Section 7.8.

Although the overwhelming majority of unstable nuclei decay by one of the mechanisms above, they do not exhaust all possibilities and in a very small number of cases other mechanisms are allowed. We will briefly mention these very rare decay modes in Section 2.6.2 and Chapter 9.

2.5 Radioactive Decay

Before looking in more detail at different types of instability, we will consider the general formalism describing the rate of radioactive decay. The probability per unit time that a given nucleus will decay is called its *decay constant* λ and is related to the *activity* $\mathcal{A}$ by

$$\mathcal{A} = -\mathrm{d}N/\mathrm{d}t = \lambda N, \tag{2.61}$$

where $N(t)$ is the number of radioactive nuclei in the sample at time t. The activity is measured in becquerels (Bq), which is defined as one decay per second.[17] The probability here refers to the total probability, because λ could be the sum of decay probabilities for a number of distinct final states in the same way that the total decay width of an unstable particle is the sum of its partial widths. Integrating (2.61) gives

$$\mathcal{A}(t) = \lambda N_0 \exp(-\lambda t), \tag{2.62}$$

where N_0 is the initial number of nuclei, i.e. the number at $t = 0$.

[17] An older unit, the curie (1 Ci $= 3.7 \times 10^{10}$ Bq) is also still in common use. A typical laboratory radioactive source has an activity of a few tens of kBq, i.e. μCi.

The *mean lifetime* τ of an unstable state, such as a radioactive nucleus or a hadron, follows from the general definition of a mean $\bar{x}$ of a distribution $f(x)$:

$$\bar{x} \equiv \left(\int x f(x)\,\mathrm{d}x\right) \Big/ \left(\int f(x)\,\mathrm{d}x\right). \tag{2.63}$$

Thus

$$\tau \equiv \frac{\int t\,\mathrm{d}N(t)}{\int \mathrm{d}N(t)} = \frac{\int_0^\infty t\exp(-\lambda t)\,\mathrm{d}t}{\int_0^\infty \exp(-\lambda t)\,\mathrm{d}t} = \frac{1}{\lambda}. \tag{2.64}$$

This is the quantity we called 'the lifetime' in Chapter 1. The mean lifetime is always used in particle physics, but another measure more commonly used in nuclear physics is the *half-life* $t_{1/2}$, defined as the time for half the number of nuclei to decay. Thus $t_{1/2} = \ln 2/\lambda = \tau \ln 2$. In this book, the term *lifetime* will be used for the mean lifetime, both for radioactive nuclei and unstable hadrons, unless explicitly stated otherwise.

A well-known use of the radioactive decay law is in dating ancient specimens using the known properties of radioactive nuclei. For organic specimens, carbon is usually used. Carbon-14 is a radioactive isotope of carbon that is produced by the action of cosmic rays on nitrogen in the atmosphere.[18] If the flux of cosmic rays remains roughly constant over time, then the ratio of ^{14}C to the stable most abundant isotope ^{12}C reaches an equilibrium value of about 1:10^{12}. Both isotopes will be taken up by living organisms in this ratio, but when the organism dies there is no further interaction with the environment and the ratio slowly changes with time as the ^{14}C nuclei decay by β decay to ^{14}N with a lifetime of 8.27×10^3 y. Thus, if the ratio of ^{14}C to ^{12}C is measured, the age of the specimen may be estimated.[19] The actual measurements can be made very accurately because modern mass spectrometers can directly measure very small differences in the concentrations of ^{14}C and ^{12}C using only milligrams of material. Nevertheless, in practice, corrections are made to agree with independent calibrations if possible, because cosmic ray activity is not strictly constant with time.

In many cases the products of radioactive decay are themselves radioactive and so a decay chain results. Consider a decay chain $A \to B \to C \to \cdots$, with decay constants $\lambda_A, \lambda_B, \lambda_C$ etc. The variation of species A with time is given by (2.62), i.e.

$$N_A(t) = N_A(0)\exp(-\lambda_A t), \tag{2.65}$$

but the differential equation for $N_B(t)$ will have an extra term in it to take account of the production of species B from the decay of species A:

$$\mathrm{d}N_B(t)/\mathrm{d}t = -\lambda_B N_B + \lambda_A N_A. \tag{2.66}$$

[18] Cosmic rays are high-energy particles, mainly protons, that impinge on the Earth's atmosphere from space. The products of the secondary reactions they produce may be detected at the Earth's surface. Victor Hess shared the 1936 Nobel Prize in Physics for the discovery of cosmic radiation.

[19] This method of using radioactive carbon to date ancient objects was devised by Willard Libby, for which he received the 1960 Nobel Prize in Chemistry.

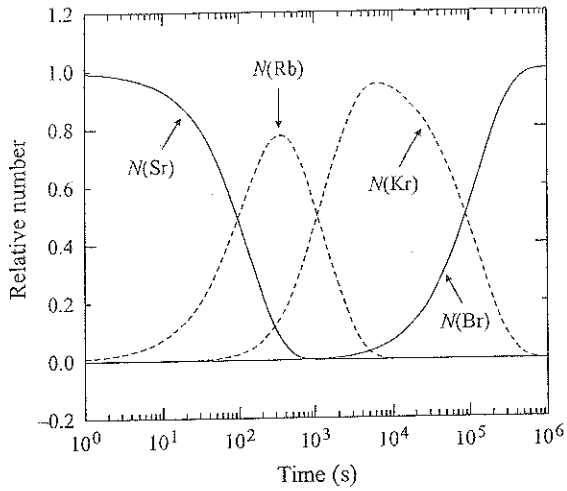

Figure 2.13 Time variation of the relative numbers of nuclei in the decay chain (2.69).

The solution of this equation may be verified by substitution to be

$$N_B(t) = \frac{\lambda_A}{\lambda_B - \lambda_A} N_A(0)[\exp(-\lambda_A t) - \exp(-\lambda_B t)]. \tag{2.67}$$

Similar equations may be found for decay sequences with more than two stages. Thus, for a three-stage sequence

$$N_C(t) = \lambda_A \lambda_B N_A(0) \times \left[\frac{\exp(-\lambda_A t)}{(\lambda_B - \lambda_A)(\lambda_C - \lambda_A)} + \frac{\exp(-\lambda_B t)}{(\lambda_A - \lambda_B)(\lambda_C - \lambda_B)} + \frac{\exp(-\lambda_C t)}{(\lambda_A - \lambda_C)(\lambda_B - \lambda_C)} \right]. \tag{2.68}$$

The time dependence of the relative sizes of the various components depends of course on the relative sizes of the decay constants.

As an example, the variation of the components as a function of time is shown in Figure 2.13 for the specific case:

$$\begin{aligned} {}^{79}_{38}\mathrm{Sr} &\rightarrow {}^{79}_{37}\mathrm{Rb} + e^+ + \nu_e \qquad (2.25 \text{ min}) \\ &\hookrightarrow {}^{79}_{36}\mathrm{Kr} + e^+ + \nu_e \qquad (22.9 \text{ min}) \\ &\hookrightarrow {}^{79}_{35}\mathrm{Br} + e^+ + \nu_e \qquad (35.04 \text{ hr}) \end{aligned} \tag{2.69}$$

Here $\lambda_A > \lambda_B > \lambda_C$ and the final nucleus is stable. This illustrates the general features for this type of sequence, that whereas $N_A(t)$ for the initial species falls monotonically with time and $N_D(t)$ for the final stable species rises monotonically, $N_B(t)$ and $N_C(t)$ for the intermediate species rise to maxima before falling. Note that at any time the sum of the components is a constant, as expected.

In the following sections we consider the phenomenology of some of the various types of radioactivity in more detail and in Chapter 7 we will return to discuss various models and theories that provide an understanding of these phenomena.

and may be unsuitable if applied to a different set of phenomena. As knowledge evolves, it is natural to try and incorporate more phenomena by modifying the model to become more general, until (hopefully) we have a model with firm theoretical underpinning that describes a very wide range of phenomena, i.e. a *theory*. The collective model, which uses the ideas of both the shell and liquid drop models, is a step in this direction.

We will conclude this part of the chapter with a very brief summary of the assumptions of each of the nuclear models we have discussed and what each can tell us about nuclear structure.

Liquid drop model: This model assumes that all nuclei have similar mass densities, with binding energies approximately proportional to their masses, just as in a classical charged liquid drop. The model leads to the SEMF, which gives a good description of the average masses and binding energies. It is largely classical, with some quantum mechanical terms (the asymmetry and pairing terms) inserted in an ad hoc way. Input from experiment is needed to determine the coefficients of the SEMF.

Fermi gas model: The assumption here is that nucleons move independently in a net nuclear potential. The model uses quantum statistics of a Fermi gas to predict the depth of the potential and the asymmetry term of the SEMF.

Shell model: This is a fully quantum mechanical model that solves the Schrödinger equation with a specific spherical nuclear potential. It makes the same assumptions as the Fermi gas model about the potential, but with the addition of a strong spin-orbit term. It is able to successfully predict nuclear magic numbers, spins and parities of ground state nuclei and the pairing term of the SEMF. It is less successful in predicting magnetic moments.

Collective model: This is also a fully quantum mechanical model, but in this case the potential is allowed to undergo deformations from the strictly spherical form used in the shell model. The result is that the model can predict magnetic dipole and electric quadrupole magnetic moments with some success. Additional modes of excitation, both vibrational and rotational, are possible and are generally confirmed by experiment.

It is clear from the above that there is at present no universal nuclear model. What we currently have is a number of models and theories that have limited domains of applicability and even within which they are not always able to explain all the observations. For example, the shell model, while able to give a convincing account of the spins and parities of the ground states of nuclei, is unable to predict the spins of excited states with any real confidence. And of course the shell model has absolutely nothing to say about whole areas of nuclear physics phenomena. Some attempt has been made to combine features of different models, such as is done in the collective model, with some success. A more fundamental theory will require the full apparatus of many-body theory applied to interacting nucleons and some progress has been made in this direction for light nuclei, as we will mention in Chapter 9. A theory based on interacting quarks is a more distant goal.

7.6 α Decay

To discuss alpha decays, we could return to the semiempirical mass formula of Chapter 2 and by taking partial derivatives with respect to A and Z find the limits of α stability, but the result is not very illuminating. To get a very rough idea of the stability criteria,

we can write the SEMF in terms of the binding energy B. Then α decay is energetically allowed if

$$B(2,4) > B(Z,A) - B(Z-2, A-4). \tag{7.41}$$

If we now make the *approximation* that the line of stability is $Z = N$ (the actual line of stability deviates from this, see Figure 2.12), then there is only one independent variable. If we take this to be A, then

$$B(2,4) > B(Z,A) - B(Z-2, A-4) \approx 4\frac{\mathrm{d}B}{\mathrm{d}A}, \tag{7.42}$$

and we can write

$$4\frac{\mathrm{d}B}{\mathrm{d}A} = 4\left[A\frac{\mathrm{d}(B/A)}{\mathrm{d}A} + \frac{B}{A}\right]. \tag{7.43}$$

From the plot of B/A (Figure 2.8), we have $\mathrm{d}(B/A)/\mathrm{d}A \approx -7.7 \times 10^{-3}$ MeV for $A \geq 120$ and we also know that $B(2,4) = 28.3$ MeV, so we have

$$28.3 \approx 4(B/A - 7.7 \times 10^{-3} A), \tag{7.44}$$

which is a straight line on the B/A versus A plot which cuts the plot at $A \approx 151$. Above this value of A the inequality (7.41) is satisfied by most nuclei and α decay becomes energetically possible.

Lifetimes of α emitters span an enormous range, and examples are known from 10 ns to 10^{17} yrs. The origin of this large spread lies in the quantum mechanical phenomenon of *tunelling*. Individual protons and neutrons have binding energies in nuclei of about 7–8 MeV, even in heavy nuclei (see Figure 2.8), and so cannot in general escape. However, a bound group of nucleons can sometimes escape because its binding energy increases the total energy available for the process. In practice, the most significant decay process of this type is the emission of an α particle, because unlike systems of 2 and 3 nucleons it is very strongly bound by 7 MeV/nucleon. Figure 7.8 shows the potential energy of an α particle as a function of r, its distance from the centre of the nucleus.

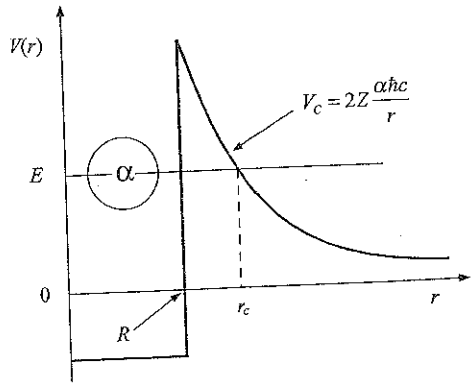

Figure 7.8 Schematic diagram of the potential energy of an α particle as a function of its distance r from the centre of the nucleus.

Beyond the range of the nuclear force, $r > R$, the α particle feels only the Coulomb potential

$$V_C(r) = \frac{2Z\alpha\hbar c}{r}, \tag{7.45}$$

where we now use Z to be the atomic number of the *daughter* nucleus. Within the range of the nuclear force, $r < R$, the strong nuclear potential prevails, with its strength characterized by the depth of the well. Since the α particle can escape from the nuclear potential, this implies that $E_\alpha > 0$. It is this energy that is released in the decay. Unless E_α is larger than the Coulomb barrier (in which case the decay would be so fast as to be unobservable) the only way the α particle can escape is by quantum mechanical tunelling through the barrier.

The probability T for transmission through a barrier of height V and thickness Δr by a particle of mass m with energy E_α is given approximately by

$$T \approx e^{-2\kappa\,\Delta r}, \tag{7.46}$$

where $\hbar\kappa = (2m|V_C - E_\alpha|)^{1/2}$. Using this result, we can model the Coulomb barrier as a succession of thin barriers of varying height. The overall transmission probability is then

$$T = e^{-G}, \tag{7.47}$$

where the *Gamow factor* G is

$$G = \frac{2}{\hbar}\int_R^{r_c} [2m|V_C(r) - E_\alpha|]^{1/2}\,\mathrm{d}r, \tag{7.48}$$

with $\beta = v/c$ and v is the velocity of the emitted particle.[14] This assumes that the orbital angular momentum of the α particle is zero, i.e. we ignore possible centrifugal barrier corrections.[15] Since r_C is the value of r where $E_\alpha = V_C(r_C)$,

$$r_C = 2Ze^2/4\pi\varepsilon_0 E_\alpha \tag{7.49}$$

and hence

$$V_C(r) = 2Ze^2/4\pi\varepsilon_0 r = r_C E_\alpha/r. \tag{7.50}$$

So, substituting into (7.48) gives

$$G = \frac{2(2mE_\alpha)^{1/2}}{\hbar}\int_R^{r_c} \left(\frac{r_C}{r} - 1\right)^{1/2}\mathrm{d}r, \tag{7.51}$$

[14] The results (7.46)–(7.48) are derived in Section A.1 of Appendix A.

[15] The existence of an angular momentum barrier will suppress the decay rate (i.e. increase the lifetime) compared to a similar nucleus without such a barrier. Numerical estimates of the suppression factors, which increase rapidly with angular momentum, have been calculated by Blatt and Weisskopf and are given in Blatt and Weisskopf (1952).

where m is the reduced mass of the α particle and the daughter nucleus, i.e. $m = m_\alpha m_D/(m_\alpha + m_D) \approx m_\alpha$. Evaluating the integral (7.51) gives

$$G = 4Z\alpha\left(\frac{2mc^2}{E_\alpha}\right)^{1/2}\left[\left(\cos^{-1}\sqrt{\frac{R}{r_C}}\right) - \sqrt{\frac{R}{r_C}\left(1-\frac{R}{r_C}\right)}\right]. \tag{7.52a}$$

Finally, since E_α is typically 5 MeV and the height of the barrier is typically 40 MeV, $r_C \gg R$ and from (7.52a),

$$G \approx 4\pi\alpha Z/\beta, \tag{7.52b}$$

where $\beta = \upsilon_\alpha/c$ and υ_α is the velocity of the α particle within the nucleus.

The probability per unit time λ of the α particle escaping from the nucleus is proportional to the product of: (a) the probability $w(\alpha)$ of finding the α particle in the nucleus; (b) the frequency of collisions of the α particle with the barrier (this is $\upsilon_\alpha/2R$); and (c) the transition probability. Combining these factors, λ is given by

$$\lambda = w(\alpha)\frac{\upsilon_\alpha}{2R}e^{-G} \tag{7.53}$$

and since

$$G \propto \frac{Z}{\beta} \propto \frac{Z}{\sqrt{E_\alpha}}, \tag{7.54}$$

small differences in E_α have strong effects on the lifetime.

To examine this further we can take logarithms of (7.53) to give

$$\log_{10} t_{1/2} = a + bZE_\alpha^{-1/2}, \tag{7.56}$$

where $t_{1/2}$ is the half-life. The quantity a depends on the probability $w(\alpha)$ and so is a function of the nucleus, whereas b is a constant that may be estimated from the above equations to be about 1.7. Equation (7.56) is a form of a relation that was found empirically by Geiger and Nuttall in 1911 long before its theoretical derivation in 1928. It is therefore called the *Geiger-Nuttall relation*. It predicts that for fixed Z, the log of the half-life of alpha emitters varies linearly with $E_\alpha^{-1/2}$.

Figure 7.9 shows lifetime data for the isotopes of four nuclei. The very strong variation with alpha particle energy is evident; changing E_α by a factor of about 2.5 changes the lifetime by 20 orders of magnitude. In all cases the agreement with the Geiger-Nuttall relation is very reasonable and the slopes are compatible with the estimate for b above. Thus the simple barrier penetration model is capable of explaining the very wide range of lifetimes of nuclei decaying by α emission.

7.7 β Decay

In Chapter 2 we discussed in some detail the phenomenology of β decay using the semi-empirical mass formula. In this section we return to these decays and examine their theoretical interpretation.

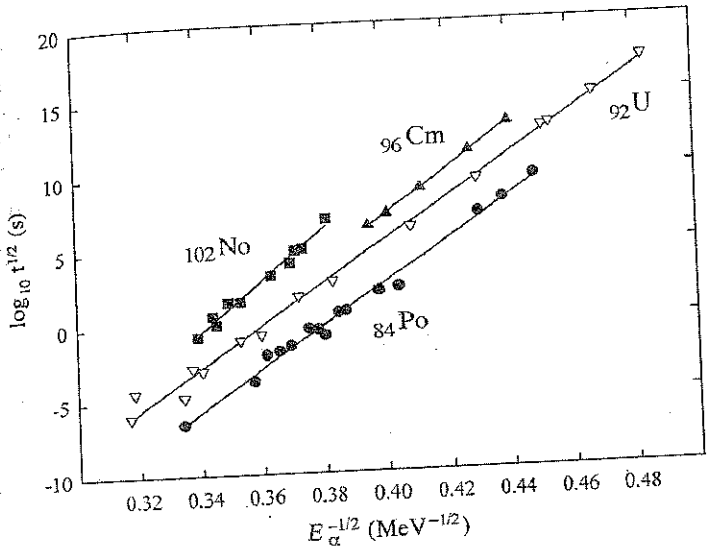

Figure 7.9 Comparison of the Geiger-Nuttall relation with experimental data for some α-emitters.

7.7.1 Fermi Theory

The first successful theory of nuclear beta decay was proposed in 1934 by Fermi. He constructed a theory based on very general principles, working by analogy with the theory of electromagnetic processes, the only successful theory known at the time for quantum particles. In electromagnetism, the interaction is described by a Lorentz-invariant scalar transition amplitude and Fermi assumed that the weak decay $i \rightarrow f$ could similarly be written:

$$\mathcal{M}_{fi} = \int \Psi_f^*(g\hat{O})\Psi_i \, \mathrm{d}V, \tag{7.57}$$

where Ψ_f and Ψ_i are total wave-functions for the final and initial states, respectively, g is a dimensionless coupling constant, and the integral is over the nuclear volume V. The interaction operator $\hat{O}$ can in principle be a combination five basic Lorentz-invariant forms. The five categories are called *scalar* (S), *pseudo-scalar* (P), *vector* (V), *axial-vector* (A), and *tensor* (T); the names having their origin in the mathematical transformation properties of the operators. Fermi guessed that $\hat{O}$ would be of the vector type, since electromagnetism is a vector interaction, i.e. it is transmitted by a spin-1 particle – the photon. The resulting $\mathbf{V} \cdot \mathbf{V}$ transitions, are called called *Fermi transitions*. However, we have seen from the work of Chapter 6 that the weak interaction does not conserve parity and so $|\mathcal{M}_{fi}|^2$ must be a mixture of a scalar and a pseudoscalar. Several combinations of operators are in principle possible, but the only one that yields the correct helicity properties for leptons is a mixture of V and A. For purely leptonic decays, the combination is **V-A**, but in the case of nuclear β decays the relative strength of the two terms has to be determined by experiment, because nuclei are extended objects. Decays proceeding via $\mathbf{A} \cdot \mathbf{A}$ combination are called

ORTEC®

Experiment 5
Energy Loss with Heavy Charged Particles (Alphas)

Equipment Required

• ULTRA™ Charged Particle Detector model **BU-014-050-100**	• **C-29** BNC Tee Connector
• **142A** Preamplifier	• **ALPHA-PPS-115** (or 230) Portable Vacuum Pump Station
• **4001A/4002D** NIM Bin and Power Supply	• **TDS3032C** Oscilloscope with bandwidth ≥150 MHz
• **575A** Spectroscopy Amplifier	• **AF-210-A1*** consisting of 1 μCi of ^{210}Po.
• **807** Vacuum Chamber	• **01865-AB** 2.5-micron Mylar 3" X 300'
• **428** Detector Bias Supply	• **01866-AB** 3.6-micron Mylar 3" X 300'
• **480** Pulser	• **01867-AB** 6.0-micron Mylar 3" X 300'
• **EASY-MCA-8K** including a USB cable and MAESTRO software (other ORTEC MCAs may be substituted)	• **S-PK-100** incorporating 100 slide mounting frames with mounting kit (plastic frames for 35-mm photographic film); used to mount the Mylar film in thicknesses from 2.5 to 25 microns in increments of 2.5 or 3.6 microns.
• **C-36-12** RG-59A/U 75 Ω Coaxial Cable with SHV Plugs, 12-ft (3.7-m) length	• Small, flat-blade screwdriver for tuning screwdriver-adjustable controls
• **C-24-1/2** RG-62A/U 93 Ω Coaxial Cable with BNC Plugs, 0.5-ft. (15-cm) length	• Personal Computer with USB port and Windows operating system
• Two **C-24-4** RG-62A/U 93 Ω Coaxial Cables with BNC Plugs, 4-ft. (1.2-cm) length	• Access to a suitable printer for printing/plotting spectra acquired with MAESTRO.
• Two **C-24-12** RG-62A/U 93 Ω Coaxial Cables with BNC Plugs, 12-ft (3.7-m) length	

*Sources are available direct from supplier. See the ORTEC website at www.ortec-online.com/Service-Support/Library/Experiments-Radioactive-Source-Suppliers.aspx

Purpose

In this experiment the principle concern will be the rate of energy loss, dE/dx, and the range of an alpha particle as it passes through matter. The two experiments involve alpha particles passing through Mylar film and through a gas. This experiment requires the procedures developed in Experiment 4. Consequently, Experiment 4 is a prerequisite.

Relevant Information

For the purpose of studying how nuclear particles lose energy in various materials, the types of radiation can be separated into five categories according to how they interact with the material: 1) fast electrons, 2) heavy charged particles, 3) massive nuclei, and 4) neutrons. Heavy charged particles include the nuclei from the various isotopes of hydrogen and helium. For hydrogen isotopes, the ions are known as protons ($^1H^+$), deuterons ($^2H^+$), or tritons ($^3H^+$). For helium, the two ions are $^3He^{++}$ or alpha particles ($^4He^{++}$). Those heavy charged particles all tend to lose energy in a similar fashion in materials. Ionized nuclei that have a much higher mass than helium have similar interaction principles, but suffer complications from size and mass that place them in a separate class. Compared to heavy charged particles, fast electrons (or beta particles) travel much further in materials, and tend to spread out in random directions. Because they have no charge, neutrons interact in materials by causing nuclear reactions, or by billiard-ball collisions with protons in the material.

Because alpha particles are readily available from natural radioactive sources, they provide a convenient means of studying the interaction of heavy particles with materials. The alpha particle is identical with a doubly-ionized helium atom and consists of 2 protons and 2 neutrons, all tightly bound together. Alpha particles emitted by natural sources typically have energies in the range of 3 to 8 MeV. The alpha is a relatively massive nuclear particle compared with the electron (~8000 times the mass of the electron). When an alpha particle goes through matter it loses energy primarily by ionization and excitation of atoms in the material. Because the alpha particle is much more massive than the atomic electrons with which it is interacting, it travels through matter in a straight line. The energy required to strip an electron from a gas atom typically lies between 25 and 40 eV. For air, the accepted average ionization potential is 32.5 eV. Therefore, the number of ion pairs that are theoretically possible can be easily calculated. The average ionization potential, I_{av}, has been determined for a variety of materials (ref. 12).

Specific ionization is defined as the number of electron-ion pairs produced per unit path length. Specific ionization is energy dependent, because the energy of a particle affects its rate of travel through the material being ionized. Lower energy alpha particles spend more time per unit of path length than do higher energy particles. Consequently, specific ionization increases as the alpha particle loses energy and slows down. Fig. 5.1 is a typical Bragg curve showing specific ionization for alpha particles in a generic

Experiment 5
Energy Loss with Heavy Charged Particles (Alphas)

material. Past the maximum specific ionization near the end of the path, the specific ionization drops, as the alpha particle picks up electrons from the material.

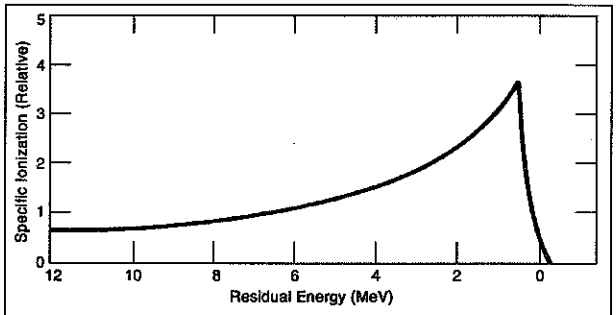

Fig. 5.1. The Bragg Curve, Illustrating Specific Ionization for an Alpha Particle.

Another parameter of vital interest is the incremental energy loss over a small increment of distance. This differential energy loss, dE/dx, is known as the stopping power for the alpha particle of energy E in a specified material. The traditional Bethe formula (ref. 3 and 11) expressing the stopping power in ergs/cm for a material composed of a single, pure element is:

$$-\frac{dE}{dx} = \frac{4\pi e^4 z^2}{m_o v^2} NB \qquad (1a)$$

Where

$$B = Z\left[ln\left(\frac{2m_o v^2}{I_{av}}\right) - ln\left(1 - \frac{v^2}{c^2}\right) - \frac{v^2}{c^2}\right] \qquad (1b)$$

where

z = the atomic number of the incident particle,
e = electronic charge (esu),
m_0 = rest mass of an electron (g),
v = the velocity of the charged particle (cm/s)
c = velocity of light (cm/s),
N = the number of atoms per cm^3 in the absorber, so that NZ is number of electrons per unit volume of absorber
I_{av} = mean ionization potential of the target (ergs),
E = energy of the incident particle (ergs).

For alpha particles having an energy <10 MeV, the velocity, v, is less than 2.3% of the speed of light. Consequently, the v^2/c^2 terms in equation (1b) are negligible, and can be ignored. Equation (1) is a seemingly simple equation that identifies the dependence of the stopping power on the charge and velocity of the charged particle, and on the atomic density and charge per atom in the absorber. The mean ionization potential, I_{av}, bears a theoretical relationship to the atoms in the absorber. But, because it is so difficult to calculate, it is generally considered a parameter that must be adjusted to fit experimental data.

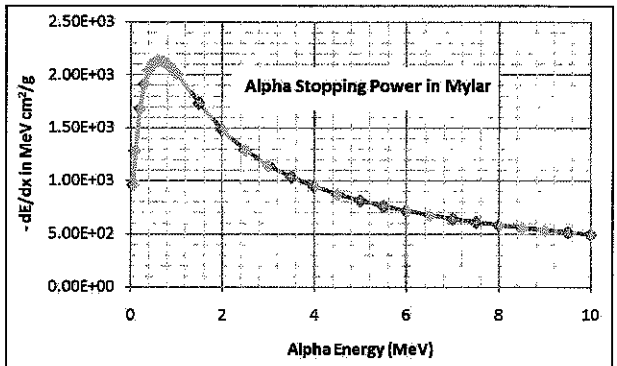

Fig. 5.2. Stopping Power for Alpha Particles in Mylar Film.

Testing the simple Bethe formula against experimental measurements shows that there are many second order effects that must be calculated and accounted for. The result is complicated, and requires a computer program to calculate the theoretical curve. Even those computer models must be fitted to experimental data at low energies. Figure 5.2 shows a calculation of the stopping power for alpha particles in Mylar (Polyethylene Terephthalate) films that has been fitted to experimental data (ref. 12). From Fig. 5.2, it can be noted that dE/dx varies slowly with energy for energies above 2 MeV.

The range of an alpha particle can be found by rearranging and integrating Equation (1) from E_0 to zero, where E_0 is the initial energy of the alpha. Fig. 5.3 is an example of the resulting range versus energy graph. Note in Fig. 5.3 that the range is expressed in g/cm^2. Expressing the range in terms of weight per unit area, instead of distance, has the benefit of allowing the curves for different absorber materials to be plotted on a more compressed vertical scale.

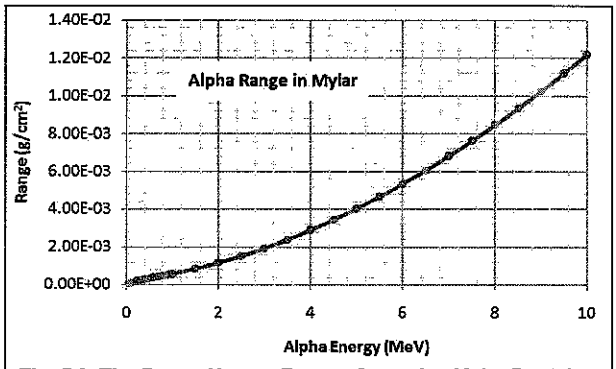

Fig. 5.3. The Range Versus Energy Curve for Alpha Particles in Mylar Film.

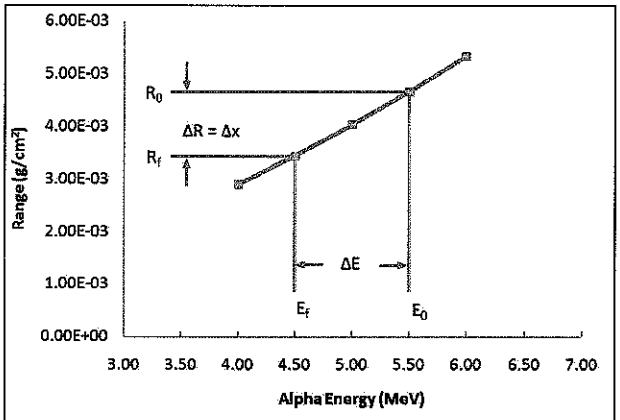

Fig. 5.4. Deriving the Energy Loss, ΔE, from the Material Thickness, Δx, using a Range-Energy Graph.

Table 5.2. Range-Energy Values for Alpha Particles in Various Absorbers (data taken from ref. 10)

	Ranges (mg/cm²)			
E_0 (MeV)	Copper	Nickel	Gold	Helium
0.25	0.79	0.74	1.31	0.181
0.50	1.09	1.02	1.90	0.245
0.75	1.38	1.29	2.50	0.316
1.00	1.69	1.58	3.12	0.399
1.25	2.01	1.88	3.79	0.490
1.50	2.36	2.21	4.47	0.601
2.00	3.11	2.91	5.97	0.850
2.50	3.93	3.68	7.59	1.14
3.00	4.82	4.50	9.34	1.48
3.50	5.80	5.44	11.00	1.86
4.00	6.81	6.39	13.10	2.29
4.50	7.90	7.40	15.20	2.76
5.00	9.10	8.51	17.40	3.27
5.50	10.30	9.66	19.70	3.82
6.00	11.60	10.87	22.10	4.41
7.00	14.30	13.46	27.10	5.70

Table 5.1 Stopping Power and Range for Alpha Particles in Mylar

Alpha Energy E_0 (MeV)	−dE/dx (MeV cm²/g)	Range (g/cm²)
5.00E−02	9.64E+02	7.69E−05
1.00E−01	1.29E+03	1.21E−04
2.00E−01	1.68E+03	1.88E−04
3.00E−01	1.91E+03	2.44E−04
4.00E−01	2.05E+03	2.94E−04
5.00E−01	2.11E+03	3.42E−04
6.00E−01	2.14E+03	3.89E−04
7.00E−01	2.13E+03	4.36E−04
8.00E−01	2.10E+03	4.83E−04
9.00E−01	2.06E+03	5.31E−04
1.00E+00	2.02E+03	5.80E−04
1.50E+00	1.73E+03	8.47E−04
2.00E+00	1.48E+03	1.16E−03
2.50E+00	1.29E+03	1.52E−03
3.00E+00	1.15E+03	1.93E−03
3.50E+00	1.04E+03	2.39E−03
4.00E+00	9.49E+02	2.90E−03
4.50E+00	8.76E+02	3.45E−03
5.00E+00	8.14E+02	4.04E−03
5.50E+00	7.62E+02	4.67E−03
6.00E+00	7.17E+02	5.35E−03
6.50E+00	6.77E+02	6.07E−03
7.00E+00	6.42E+02	6.83E−03
7.50E+00	6.11E+02	7.62E−03
8.00E+00	5.83E+02	8.46E−03
8.50E+00	5.58E+02	9.34E−03
9.00E+00	5.35E+02	1.03E−02
9.50E+00	5.14E+02	1.12E−02
1.00E+01	4.95E+02	1.22E−02

The tabular data producing Figures 5.2 and 5.3 is listed in Table 5.1. Reference 12 is an excellent source of tabulated data for Range and Stopping Power in a variety of commonly encountered materials. Table 5.1 is a compressed listing of the data from the ASTAR program offered by ref. 12.

Once the theoretical range-energy curve has been plotted, as in Figure 5.3, the energy loss, ΔE, for a given film or foil thickness, Δx, can be predicted for the initial alpha-particle energy, E_0. The principle is illustrated in Figure 5.4, which shows a small section of a range-energy curve. The original energy of the alpha particle, E_0, is used to determine the value R_0 from the curve. The thickness of the foil or film, Δx (in units of weight per unit area), is subtracted from R_0 to find R_f. In other words, $\Delta R = \Delta x$. The point on the curve determined by R_f is used to find the corresponding value, E_f, the energy with which the alpha particle exits the film. Subsequently, $\Delta E = E_0 - E_f$ predicts the energy loss as the alpha particle travels through the foil (film) of thickness, Δx.

Table 5.2 tabulates some range-energy information for copper, nickel, gold, and helium. Traditionally, copper, nickel and gold foils have been used to demonstrate range versus energy. However, these metal films are extremely thin. They are difficult to fabricate, and are easily damaged in handling. Consequently, this experiment employs readily available and rugged Mylar films.

Experiment 5
Energy Loss with Heavy Charged Particles (Alphas)

Alpha Sources

CAUTION: Alpha sources offer a potential contamination problem. Never touch the face of a source with your fingers. Most alpha sources are electrodeposited onto platinum disks. The actual radioactive source is usually a spot ~1 mm diameter deposited in the geometrical center of the disk. If you look carefully, you may be able to see the deposited spot. **ALWAYS handle an alpha source by the edge of the mounting disk.**

The 1-μCi ^{210}Po alpha source specified for this experiment has the advantage of emitting only one alpha energy (5.304 MeV). When initially purchased, it should yield a counting rate of approximately 90 counts/second with the detector and source-to-detector spacing designated in this experiment. But, its short half life (138 days) implies that it will have to be replaced each year. At the laboratory manager's discretion, an ^{241}Am source (432 year half life) could be substituted to obviate the frequent source purchases. The ^{241}Am source has the drawback that it emits three fairly closely spaced alpha energies (see Experiment 4). Although, it still should be possible to utilize the dominant 5.486 MeV peak for the energy loss measurement. The ^{241}Am alternative will make it difficult to use the data in Table 5.4 in Experiment 5.2.

It is advisable to revisit the information in Experiment 4 on the care and handling of radioactive alpha sources.

EXPERIMENT 5.1. $\Delta E/\Delta x$ for Alpha Particles in Mylar Films

NOTE: The laboratory manager will supply Mylar films of various thicknesses mounted in 35 mm slide holders. The thickness of each film should be marked on the slide frames. The thickness should increase from zero to 25 μm in approximately equal increments. The thickness increments should be in the range of 2.5 to 3.6 μm, which can be achieved by stacking multiple sheets of 2.5 micron or 3.6 micron Mylar films. To convert from microns thickness to g/cm^2, use 1.390 g/cm^3 for the density of Mylar.

Procedure

Initial Set-up

1. Connect the equipment as shown in Fig. 5.5 according to the instructions in Experiment 4.
2. Set up the controls on the instrumentation as outlined in Experiment 4, except set the amplifier gain to record the 5.48 or 5.31 MeV peak approximately in the middle of the top quadrant of the energy spectrum. Ensure that the pole-zero adjustment has been properly accomplished.

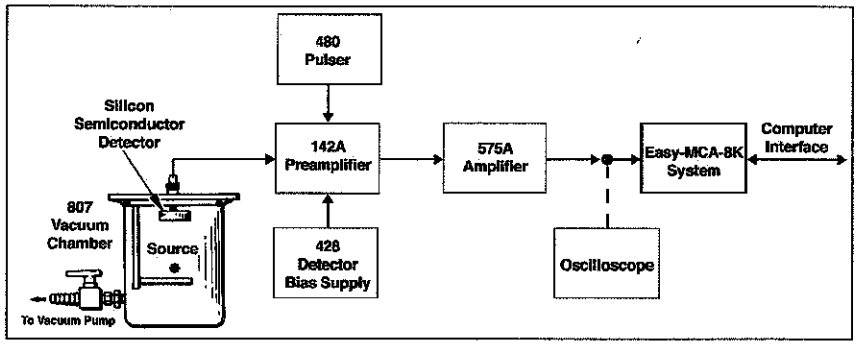

Fig. 5.5. System for the dE/dx Measurement.

3. Calibrate the system using the ^{210}Po source and the pulse generator. Using a combination of the pulser and at least one alpha source (as outlined in Experiment 4) is the most efficient method to cover the energy range from 5.5 MeV down to 1 MeV. For measurement of energy losses, it will be most convenient if the Energy Calibration feature of MAESTRO software is implemented to calibrate the horizontal scale of the multichannel analyzer. That will enable the cursor to measure the energy directly on each peak.
4. If the MAESTRO energy calibration feature has not been employed, plot the calibration curve per Experiment 4.
5. Determine the FWHM resolution of the pulser and of the alpha source as in Experiment 4.

Energy-Loss Measurements in Mylar Films

6. Turn off the pulser, lower the detector bias voltage to zero and vent the vacuum chamber to atmospheric pressure.
7. Install the ^{210}Po source in the vacuum chamber with a source-to-detector distance of approximately 4 cm. This distance must be rigidly maintained throughout the series of energy-loss measurements. Confirm that a reliable mounting system is in place for holding the Mylar films in their plastic frames between the source and the detector, with an unrestricted line of sight for the alpha particles from the source through the Mylar film to the entire sensitive area of the detector.
8. Pump a 100 micron vacuum in the chamber, and slowly raise the detector bias to its proper voltage.
9. Clear the contents of the MCA. Collect a spectrum on the bare source long enough to obtain ~4000 counts under the alpha peak. Save this spectrum on the hard disk or a transportable medium for later reference. Record the energy of the peak position, the FWHM energy resolution and the sum of the counts in the peak.

Radiation Detection and Measurement, G. F. Knoll, 3rd Ed, 2000

This definition is most commonly used in tables of numerical range values. Another version that appears in the literature is the *extrapolated range*, which is obtained by extrapolating the linear portion of the end of the transmission curve to zero.

The range of charged particles of a given energy is thus a fairly unique quantity in a specific absorber material. In the early days of radiation measurement, experiments of the type sketched in Fig. 2.5 were widely used to measure the energy of alpha particles indirectly by determining the absorber thickness equivalent to their mean range. With the availability of detectors that provide an output signal directly related to the alpha particle energy, such indirect measurements are no longer necessary.

Some graphs of the mean range of various charged particles in materials of interest in detectors are given in Figs. 2.6 through 2.8. As one obvious application of these curves, any detector that is to measure the full incident energy of a charged particle must have an active thickness that is greater than the range of that particle in the detector material.

2. *RANGE STRAGGLING*

Charged particles are also subject to *range straggling*, defined as the fluctuation in path length for individual particles of the same initial energy. The same stochastic factors that lead to energy straggling at a given penetration distance also result in slightly different

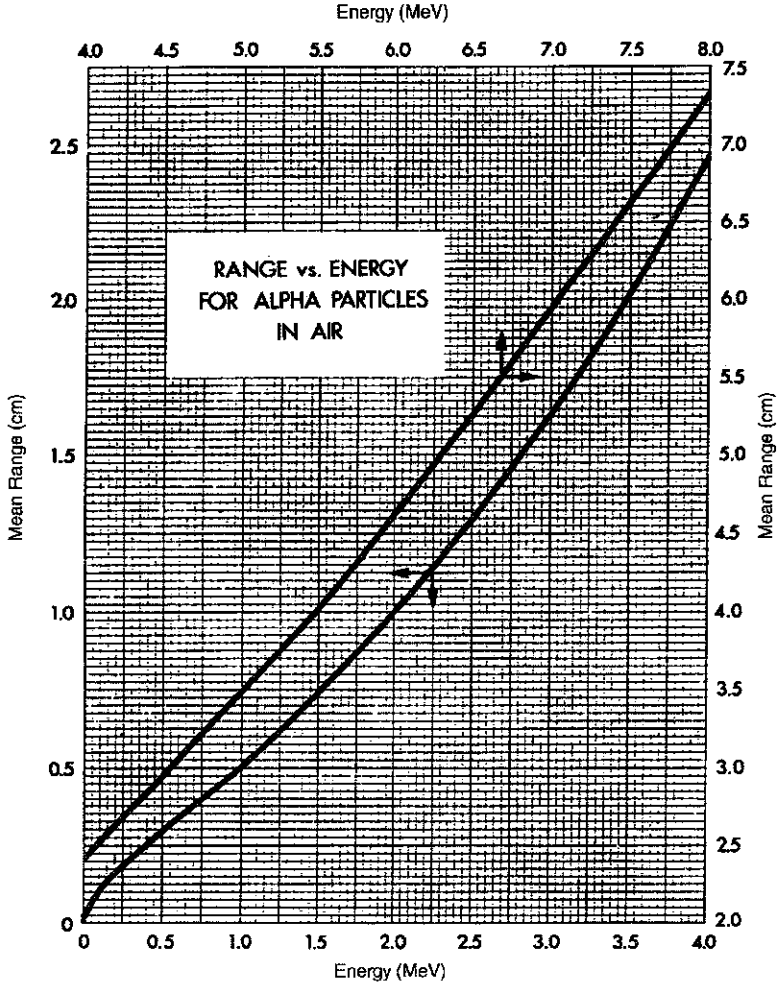

Figure 2.6 Range–energy plot for alpha particles in air at 15°C and 760 mm Hg pressure. (From *Radiological Health Handbook*, U.S. Department of Health, Education and Welfare, Washington, DC, 1970.)

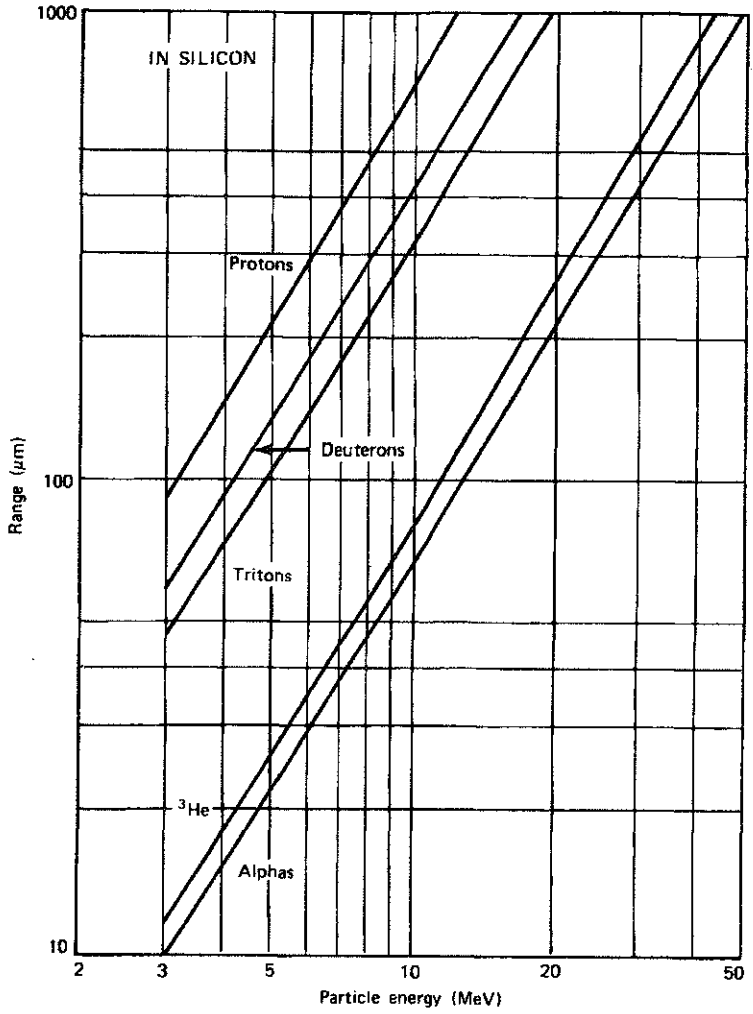

Figure 2.7 Range–energy curves calculated for different charged particles in silicon. The near-linear behavior of the log–log plot over the energy range shown suggests an empirical relation to the form $R = aE^b$, where the slope-related parameter b is not greatly different for the various particles. (From Skyrme.[4])

total path lengths for each particle. For heavy charged particles such as protons or alphas, the straggling amounts to a few percent of the mean range. The degree of straggling is evidenced by the sharpness of the cutoff at the end of the average transmission curve plotted in Fig. 2.2. Differentiating this curve leads to a peak whose width is often taken as a quantitative measure of the importance of range straggling for the particles and absorber used in the measurement.

3. STOPPING TIME

The time required to stop a charged particle in an absorber can be deduced from its range and average velocity. For nonrelativistic particles of mass m and kinetic energy E, the velocity is

$$v = \sqrt{\frac{2E}{m}} = c\sqrt{\frac{2E}{mc^2}} = \left(3.00 \times 10^8 \frac{\text{m}}{\text{s}}\right)\sqrt{\frac{2E}{(931\ \text{MeV/amu})m_A}}$$

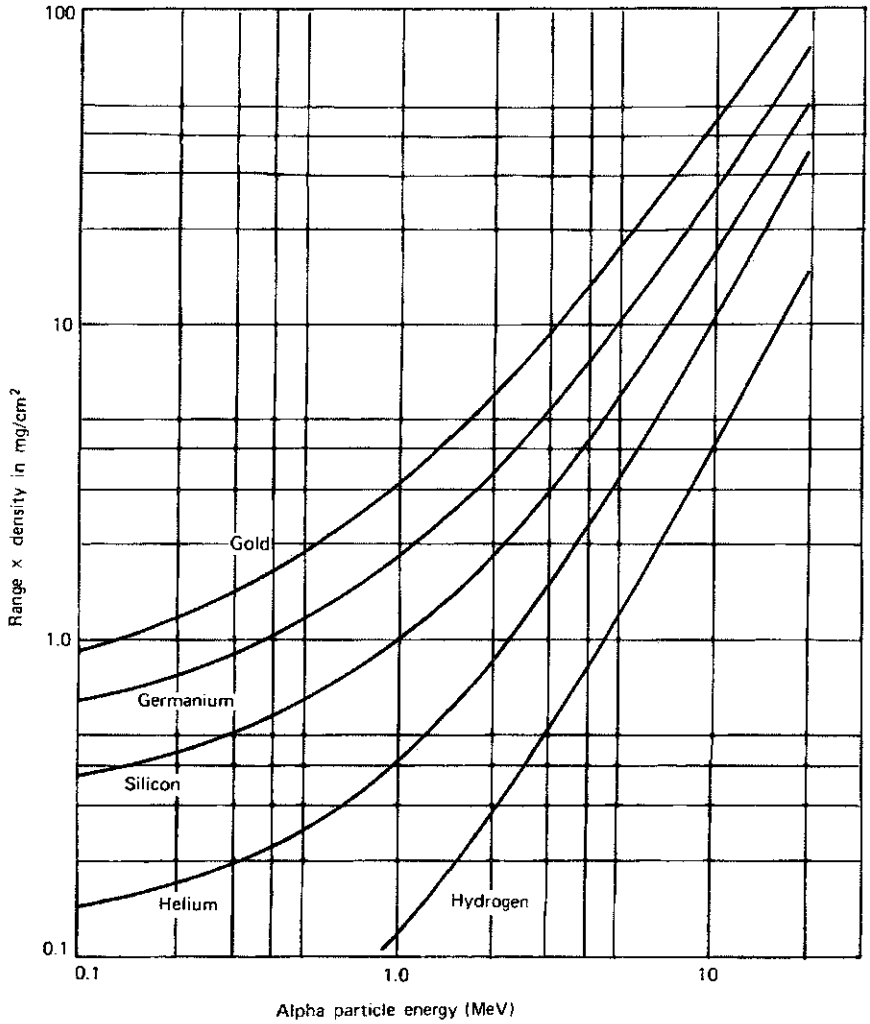

Figure 2.8 Range–energy curves calculated for alpha particles in different materials. Units of the range are given in mass thickness (see p. 54) to minimize the differences in these curves. (Data from Williamson et al.[5])

where m_A is the particle mass in atomic mass units and E is the particle energy in MeV. If we assume that the average particle velocity as it slows down is $\langle v \rangle = Kv$, where v is evaluated at the initial energy, then the stopping time T can be calculated from the range R as

$$T = \frac{R}{\langle v \rangle} = \frac{R}{Kc}\sqrt{\frac{mc^2}{2E}} = \frac{R}{K(3.00 \times 10^8\ \text{m/s})}\sqrt{\frac{931\ \text{MeV/amu}}{2}}\sqrt{\frac{m_A}{E}}$$

If the particle were uniformly decelerated, then $\langle v \rangle$ would be given by $v/2$ and K would be 0.5. However, charged particles generally lose energy at a greater rate near the end of their range, and K should be a somewhat higher fraction. By assuming $K = 0.60$, the stopping time can be estimated as

$$T \cong 1.2 \times 10^{-7} R \sqrt{\frac{m_A}{E}} \tag{2.3}$$

where T is in seconds, R in meters, m_A in amu, and E in MeV. This approximation is expected to be reasonably accurate for light charged particles (protons, alpha particles, etc.) over much of the energy range of interest here. It is not, however, to be used for relativistic particles such as fast electrons.

Using typical range values, stopping times calculated from Eq. (2.3) for charged particles are a few picoseconds in solids or liquids and a few nanoseconds in gases. These times are generally small enough to be neglected for all but the fastest-responding radiation detectors.

E. Energy Loss in Thin Absorbers

For thin absorbers (or detectors) that are penetrated by a given charged particle, the energy deposited within the absorber can be calculated from

$$\Delta E = -\left(\frac{dE}{dx}\right)_{\text{avg}} t \tag{2.4}$$

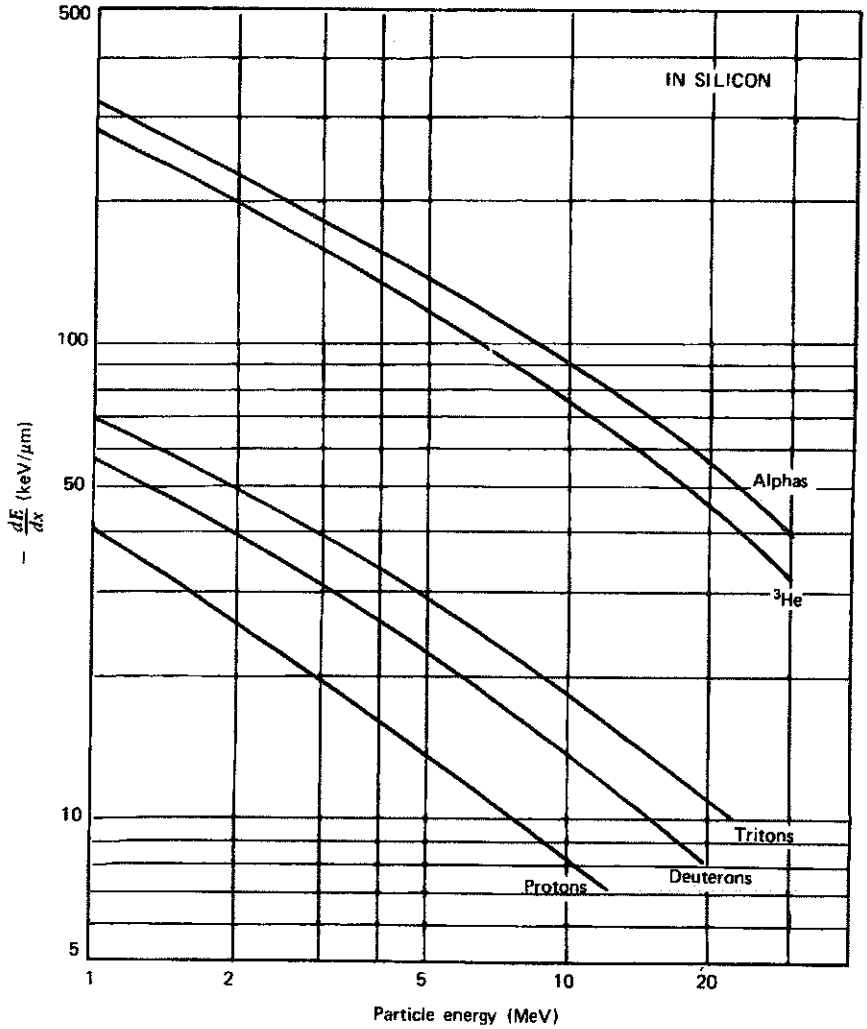

Figure 2.9 The specific energy loss calculated for different charged particles in silicon. (From Skyrme.[4])

where t is the absorber thickness and $(-dE/dx)_{avg}$ is the linear stopping power averaged over the energy of the particle while in the absorber. If the energy loss is small, the stopping power does not change much and it can be approximated by its value at the incident particle energy. Tabular values for dE/dx for a number of different charged particles in a variety of absorbing media are given in Refs. 5–10. Some graphs for materials of interest are shown in Figs. 2.9 through 2.11.

For absorber thicknesses through which the energy loss is not small, it is not simple to obtain a properly weighted $(-dE/dx)_{avg}$ value directly from such data. In these cases, it is easier to obtain the deposited energy in a way that makes use of range–energy data of the type plotted in Figs. 2.6 through 2.8. The basis of the method is as follows: Let R_1 represent the full range of the incident particle with energy E_0 in the absorber material. By subtracting the physical thickness of the absorber t from R_1, a value R_2 is obtained that represents the range of those alpha particles that emerge from the opposite surface of the absorber. By finding the energy corresponding to R_2, the energy of the transmitted charged particles

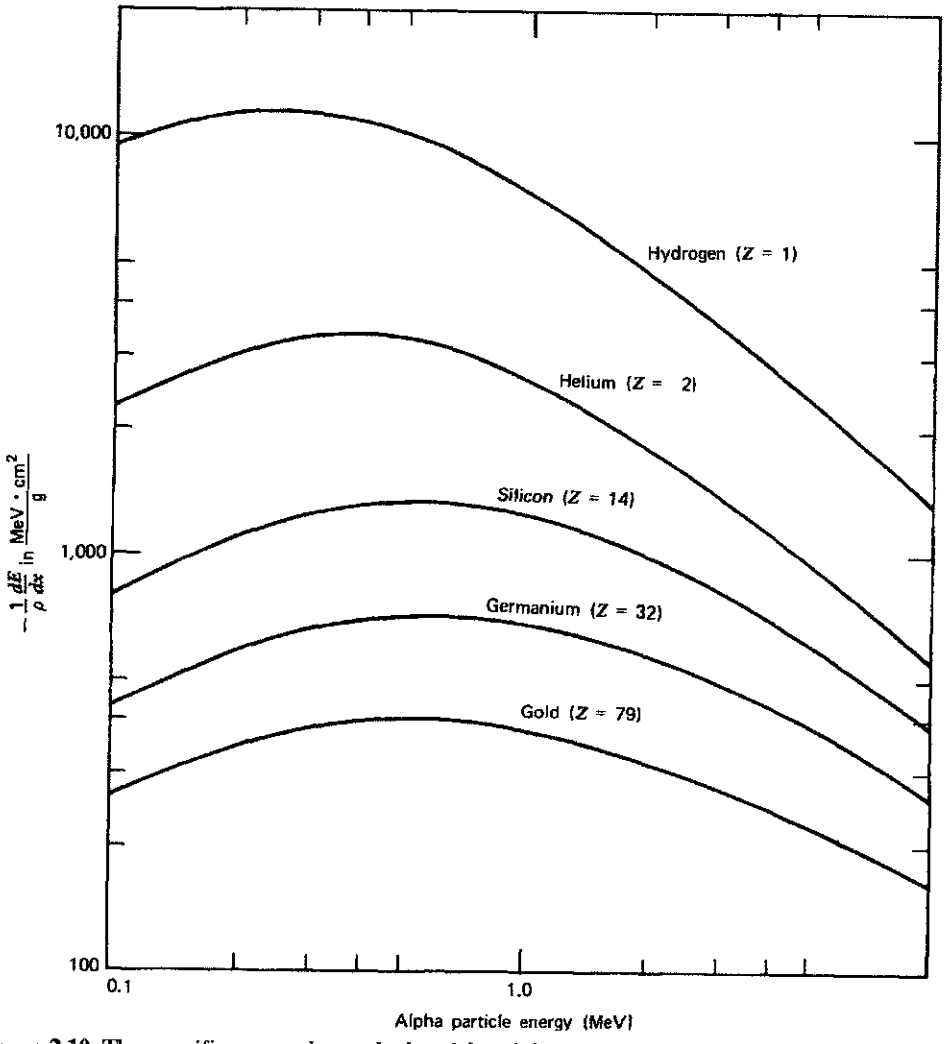

Figure 2.10 The specific energy loss calculated for alpha particles in different materials. Values are normalized by the density of the absorber material. (Data from Williamson et al.[5])

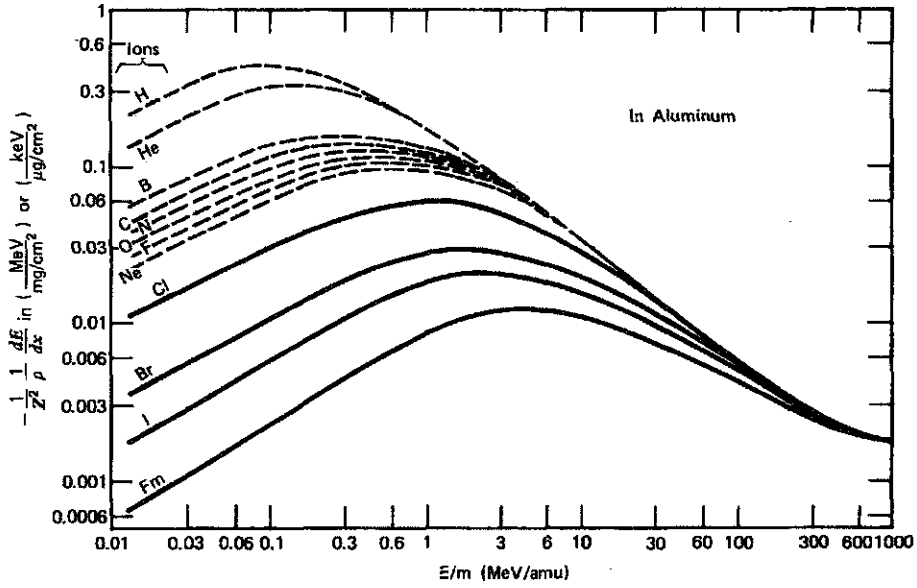

Figure 2.11 Plots showing the specific energy loss of various heavy ions in aluminum. The abscissa is the ion energy divided by its mass, and the ordinate is $-dE/dx$ divided by the density of aluminum and the square of the ion atomic number. Typical fission fragments (e.g., iodine) show a continuously decreasing $-dE/dx$ while slowing from their initial energy (~1 MeV/amu). (From Northcliffe and Schilling.[8])

E_t is obtained. The deposited energy ΔE is then given simply by $E_0 - E_t$. These steps are illustrated below:

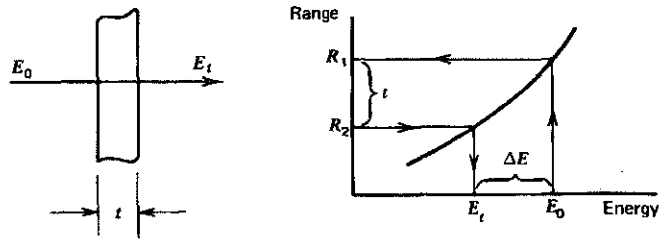

The procedure is based on the assumption that the charged particle tracks are perfectly linear in the absorber, and the method does not apply in situations where the particle can be significantly deflected (such as for fast electrons).

The combined effects of particle range and the decrease in dE/dx with increasing energy are illustrated in Fig. 2.12. Here the energy loss of protons in a thin detector is plotted versus the incident proton energy. For low energies, the proton range is less than the detector thickness. Therefore, as the energy is increased, the energy deposited in the detector (which is just equal to the incident energy) increases linearly. At a proton energy of 425 keV, the range is exactly equal to the detector thickness. For higher energies, only a portion of incident energy is deposited, and the transmitted proton carries off the remainder. Under these conditions, the energy deposited in the detector is given by Eq. (2.4), or simply the product of the detector thickness and the average linear stopping power. Because the stopping power continuously decreases with increasing energy in this region (see Fig. 2.3), the deposited energy therefore *decreases* with further increases in the

S R I M
The Stopping and Range of Ions in Matter

(Return to Home)

SRIM is a group of programs which calculate the stopping and range of ions (up to 2 GeV/amu) into matter using a quantum mechanical treatment of ion-atom collisions (assuming a moving atom as an ***"ion"***, and all target atoms as ***"atoms"***). This calculation is made very efficient by the use of statistical algorithms which allow the ion to make jumps between calculated collisions and then averaging the collision results over the intervening gap. During the collisions, the ion and atom have a screened Coulomb collision, including exchange and correlation interactions between the overlapping electron shells. The ion has long range interactions creating electron excitations and plasmons within the target. These are described by including a description of the target's collective electronic structure and interatomic bond structure when the calculation is setup (tables of nominal values are supplied). The charge state of the ion within the target is described using the concept of effective charge, which includes a velocity dependent charge state and long range screening due to the collective electron sea of the target.

A full description of the calculation is found in our tutorial book "***SRIM - The Stopping and Range of Ions in Solids***", by J. F. Ziegler and J. P. Biersack in 1985 (a new edition was published in 2009). This book presents the physics of ion penetration into solids in a simple tutorial manner, then presents the source code for SRIM programs with a full explanation of the physics. Further chapters document the accuracy of SRIM and show various applications. Available on this website are plots showing SRIM stopping powers and all available experimental data for H and He ions into all targets.

TRIM (the Transport of Ions in Matter) is the most comprehensive program included. TRIM will accept complex targets made of compound materials with up to eight layers, each of different materials. It will calculate both the final 3D distribution of the ions and also all kinetic phenomena associated with the ion's energy loss: target damage, sputtering, ionization, and phonon production. All target atom cascades in the target are followed in detail. The programs are made so they can be interrupted at any time, and then resumed later. Plots of the calculation may be saved, and displayed when needed (it takes 5 seconds to begin viewing a saved calculation).

SRIM results from the original work by J. P. Biersack on range algorithms (see J. P. Biersack and L. Haggmark, Nucl. Instr. and Meth., vol. 174, 257, 1980) and the work by J. F. Ziegler on stopping theory (see "***The Stopping and Range of Ions in Matter***", *volumes 2 - 6*, Pergamon Press, 1977-1985). The various versions of SRIM are described briefly in the file VERSION on the SRIM package.

The SRIM program originated in 1983 as a DOS based program and was converted to Windows in 1989.

If you use SRIM programs in a scientific publication, please mail a copy to the authors. This will help continued support of SRIM in the future.

(Return to Home)

it's diffused freely

EXOTIC BEAM PRODUCTION WITH FRAGMENT SEPARATORS

LISE++

Home
Introduction
Documentation
Last Changes
LISE utilities in at
Perspectives
Download
MOTER
PACE4
Spectrometers
Related topics
Personal pages
Registration
Email

v. 9.10.343

Range of application

The program **LISE++** has been developed to calculate the transmission and yields of fragments produced and collected in a spectrometer. This code allows to simulate an experiment, beginning from the parameters of the reaction mechanism and finishing with the registration of products selected by a spectrometer. The program allows to quickly optimize the parameters of the spectrometer before or during the experiment. It also makes it possible to estimate and work in conditions of maximum output of studied reaction products and their unambiguous identification. Wedge and Wien filter selections are also included in the program.

LISE++ is the new generation of the **LISE** code, which allows the creation of a spectrometer through the use of different "blocks". The number of blocks used to create a spectrometer in LISE++ is limited by operating memory of your PC and your imagination.

built-in Energy loss, Time-of-Flight, Position, Angular, Charge, Cross-Section distribution plots and dE-E, dE-TOF, Z-A/Q and dE-X two-dimensional plots allow to visualize the results of the program calculations. An application of transport integral lies in the basis of fast calculations of the program for the estimation of temporary evolution of distributions of phase space.

The LISE++ code may be applied at medium-energy and high-energy facilities (fragment- and recoil-separators with electrostatic and/or magnetic selections). A number of these facilities, like A1900 and S800 at NSCL, LISE3, SISSI/LISE3 and SPEG at GANIL, FRS and SuperFRS at GSI, RIPS and BigRIPS at RIKEN, based on the separation of projectile-like and fission fragments, fusion residues are included or might be easily added to the existing optical configuration files.

The Projectile Fragmentation, Fusion-Evaporation, Fusion-Fission, Coulomb Fission, and Abrasion-Fission assumed in this program as the production reaction mechanism allows to simulate experiments at beam energies above the Coulomb barrier.

Built-in powerful tools:

- **Monte Carlo simulation of fragment transmission,**
- **Monte Carlo simulation of fission fragment kinematics,**
- **Ion Optics calculation and Optimization** *(new)*,
- **LISE for Excel (MS Windows, Mac OS - download)**

LISE++ calculators:

- **«Physical Calculator»,**
- **«Relativistic Kinematics Calculator»,**
- **«Evaporation Calculator»,**
- **«Radiation Residue Calculator»** *(new)*,
- **«Ion Mass calculator"** *(new)*,
- **«Matrix calculator"**

Implemented codes:

- **«PACE4» (fusion-evaporation code),**
- **«MOTER» (raytracing-type program for magnetic optic system design)**
- **«ETACHA4» (charge-state distribution code)** *(new)*,
- **«Global» (charge-state distribution code),**
- **«Charge» (charge-state distribution code),**
- **«Spectroscopic Calculator" (of J.Kantele»)**

LISE++ Utilities:

- **Stripper Foil Lifetime Utility,**
- **Brho Analyzer,**
- **Twinsol (solenoid) utility,**
- **Units Converter,**
- **ISOL Catcher,**
- **Decay Analysis** (includes Proton, Alpha, Cluster, Sp.Fission half-lives calculation),
- **Reaction Utilities** (Characteristics, Converters, Plots),
- **«BI»**- the automatized search of two-dimensional peaks in spectra

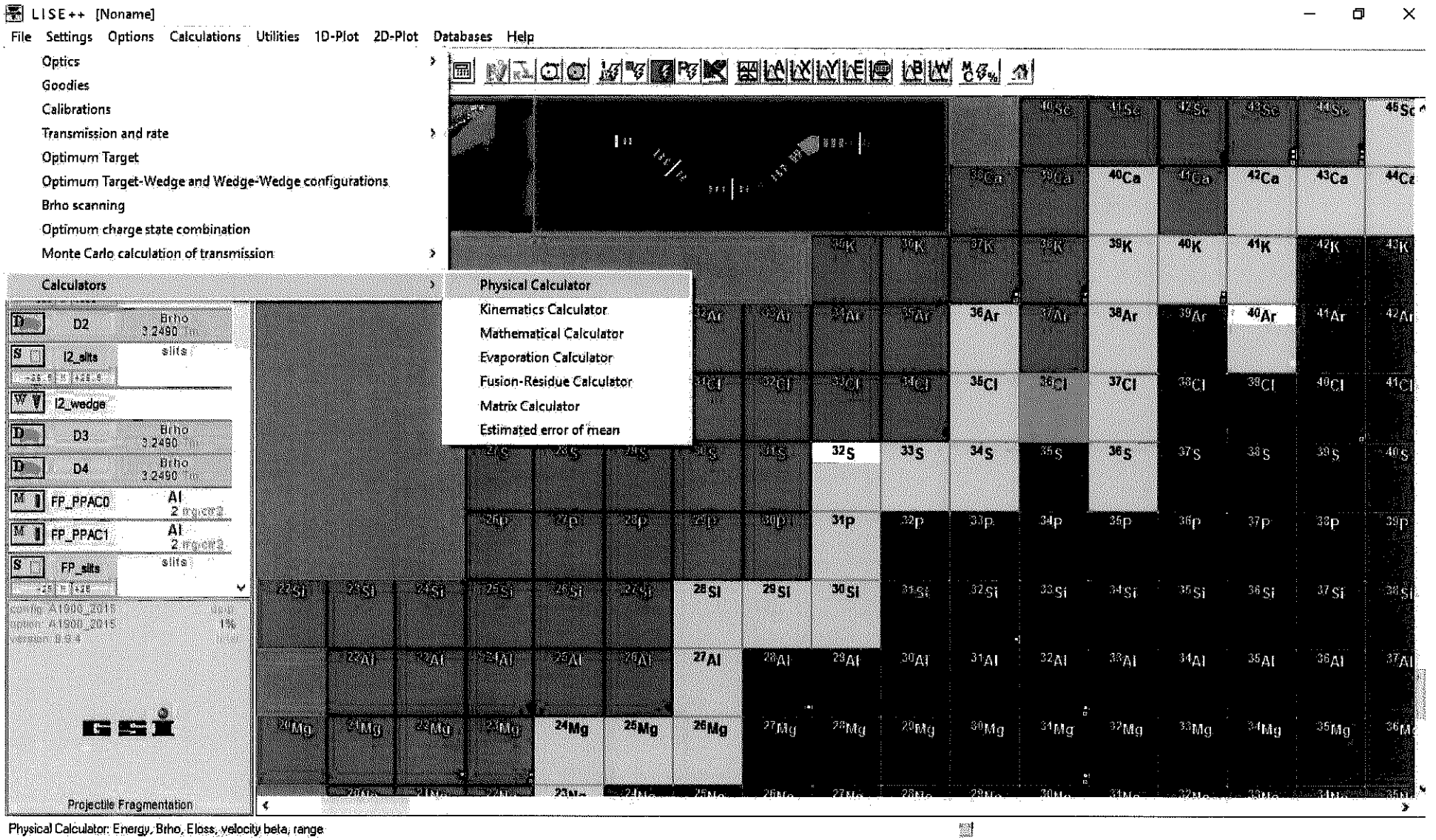
LISE++ [Noname]
File Settings Options Calculations Utilities 1D-Plot 2D-Plot Databases Help
Optics
Goodies
Calibrations
Transmission and rate
Optimum Target
Optimum Target-Wedge and Wedge-Wedge configurations
Brho scanning
Optimum charge state combination
Monte Carlo calculation of transmission
Calculators
Physical Calculator
Kinematics Calculator
Mathematical Calculator
Evaporation Calculator
Fusion-Residue Calculator
Matrix Calculator
Estimated error of mean
D2
I2_slits
I2_wedge
D3
D4
FP_PPAC0
FP_PPAC1
FP_slits
GSI
Projectile Fragmentation
Physical Calculator: Energy, Brho, Eloss, velocity beta, range

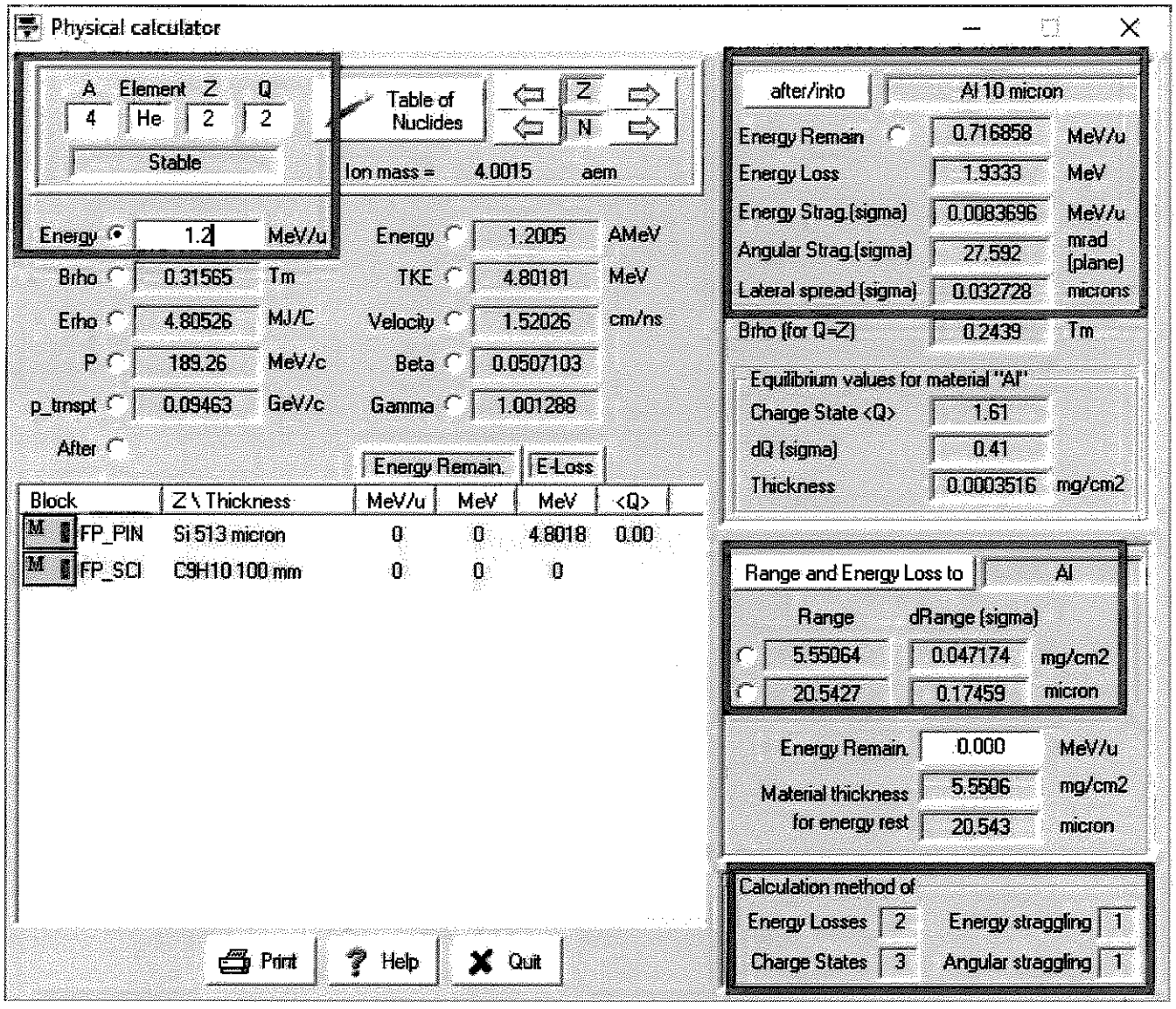
Physical calculator
A Element Z Q
4 He 2 2
Stable
Table of Nuclides
Z
N
Ion mass = 4.0015 aem
Energy 1.2 MeV/u
Energy 1.2005 AMeV
Brho 0.31565 Tm
TKE 4.80181 MeV
Erho 4.80526 MJ/C
Velocity 1.52026 cm/ns
P 189.26 MeV/c
Beta 0.0507103
p_trnspt 0.09463 GeV/c
Gamma 1.001288
After
Energy Remain.
E-Loss
Block
Z \ Thickness
MeV/u
MeV
MeV
<Q>
M FP_PIN Si 513 micron 0 0 4.8018 0.00
M FP_SCI C9H10 100 mm 0 0 0
Print
Help
Quit
after/into
Al 10 micron
Energy Remain 0.716858 MeV/u
Energy Loss 1.9333 MeV
Energy Strag.(sigma) 0.0083696 MeV/u
Angular Strag.(sigma) 27.592 mrad (plane)
Lateral spread (sigma) 0.032728 microns
Brho (for Q=Z) 0.2439 Tm
Equilibrium values for material "Al"
Charge State <Q> 1.61
dQ (sigma) 0.41
Thickness 0.0003516 mg/cm2
Range and Energy Loss to
Al
Range
dRange (sigma)
5.55064 0.047174 mg/cm2
20.5427 0.17459 micron
Energy Remain. 0.000 MeV/u
Material thickness for energy rest 5.5506 mg/cm2
20.543 micron
Calculation method of
Energy Losses 2
Energy straggling 1
Charge States 3
Angular straggling 1

Techniques for Nuclear and Particle Physics, W.R. Leo, 1987

2. Passage of Radiation Through Matter

This chapter concerns the basic reactions which occur when radiation encounters matter and the effects produced by these processes. For the experimental nuclear or particle physicist, knowledge of these interactions is of paramount importance. Indeed, as will be seen in the following chapters, these processes are the basis of all current particle detection devices and thus determine the sensitivity and efficiency of a detector. At the same time, these same reactions may also interfere with a measurement by disturbing the physical state of the radiation: for example, by causing energy information to be lost, or deflecting the particle from its original path, or absorbing the particle before it can be observed. A knowledge of these reactions and their magnitudes is thus necessary for experimental design and corrections to data. Finally, these are also the processes which occur when living matter is exposed to radiation.

Penetrating radiation, of course, sees matter in terms of its basic constituents, i.e., as an aggregate of electrons and nuclei (and their constituents as well!). Depending on the type of radiation, its energy and the type of material, reactions with the atoms or nuclei as a whole, or with their individual constituents may occur through whatever channels are allowed. An alpha particle entering a gold foil, for example, may scatter elastically from a nucleus via the Coulomb force, or collide electromagnetically with an atomic electron, or be absorbed in a nuclear reaction to produce other types of radiation, among other processes. These occur with a certain probability governed by the laws of quantum mechanics and the relative strengths of the basic interactions involved. For charged particles and photons, the most common processes are by far the electromagnetic interactions, in particular, inelastic collisions with the atomic electrons. This is not too surprising considering the strength and long range of the Coulomb force relative to the other interactions. For the the neutron, however, processes involving the strong interaction will preferentially occur, although it is also subject to electromagnetic (through its magnetic moment!) and weak processes as well. The type of processes allowed to each type of radiation explain, among other things, their penetrability through matter, their difficulty or ease of detection, their danger to biological organisms, etc.

The theory behind the principal electromagnetic and neutron processes is well developed and is covered in many texts on experimental nuclear and particle physics. In this chapter, therefore, we will only briefly survey the relevant ideas and concentrate instead on those results useful for nuclear and particle physics. As well, we restrict ourselves only to the energy range of nuclear and particle physics, i.e., a few keV and higher.

2.1 Preliminary Notions and Definitions

To open our discussion of radiation in matter, we first review a few basic notions concerning the interaction of particles.

2.1.1 The Cross Section

The collision or interaction of two particles is generally described in terms of the *cross section*. This quantity essentially gives a measure of the probability for a reaction to occur and may be calculated if the form of the basic interaction between the particles is known. Formally, the cross-section is defined in the following manner. Consider a beam of particles *1* incident upon a target particle *2* as shown in Fig. 2.1. Assume that the beam is much broader than the target and that the particles in the beam are uniformly distributed in space and time. We can then speak of a *flux* of F incident particles per unit area per unit time. Now look at the number of particles scattered[1] into the solid angle $d\Omega$ per unit time. Because of the randomness of the impact parameters, this number will fluctuate over different finite periods of measuring time. However, if we average many finite measuring periods, this number will tend towards a fixed $dN_s/d\Omega$, where N_s is the average number scattered per unit time. The *differential* cross section is then defined as the ratio

$$\frac{d\sigma}{d\Omega}(E, \Omega) = \frac{1}{F}\frac{dN_s}{d\Omega}, \tag{2.1}$$

that is, $d\sigma/d\Omega$ is the average fraction of the particles scattered into $d\Omega$ per unit time per unit flux F. In terms of a single quantum mechanical particle, this may be reformulated as the scattered probability current in the angle $d\Omega$ divided by the total incident probability passing through a unit area in front of the target.

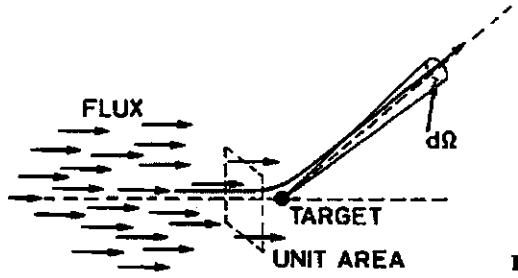

Fig. 2.1. Definition of the scattering cross section

Note that because of the dimensions of F, $d\sigma$ has dimensions of area, which leads to the heuristic interpretation of $d\sigma$ as the geometric cross sectional area of the target intercepting the beam. That fraction of the flux incident on this area will then obviously interact while all those missing $d\sigma$ will not. This is only a visual aid, however, and should in *no* way be taken as a real measure of the physical dimensions of the target.

In general, the value of $d\sigma/d\Omega$ will vary with the energy of the reaction and the angle at which the particle is scattered. We can calculate a *total* cross section for any scattering whatsoever at an energy E defined as the integral of $d\sigma/d\Omega$ over all solid angles,

$$\sigma(E) = \int d\Omega \frac{d\sigma}{d\Omega}. \tag{2.2}$$

[1] By *scattering* here, we mean *any* reaction in which an outgoing particle is emitted into Ω. The incident particle need not retain its identity.

While the above example is easily visualized, it is not a practical case. In real situations, of course, the target is usually a slab of material containing many scattering centers and it is desired to know how many interactions occur on the average. Assuming that the target centers are uniformly distributed and the slab is not too thick so that the likelihood of one center sitting in front of another is low, the number of centers per unit perpendicular area which will be seen by the beam is then $N\,\delta x$ where N is the density of centers and δx is the thickness of the material along the direction of the beam. If the beam is broader than the target and A is the total perpendicular area of the target, the number of incident particles which are eligible for an interaction is then FA. The average number scattered into $d\Omega$ per unit time is then

$$N_s(\Omega) = FA\,N\,\delta x \frac{d\sigma}{d\Omega}. \tag{2.3}$$

The total number scattered into all angles is similarly

$$N_{\text{tot}} = FA\,N\,\delta x\,\sigma. \tag{2.4}$$

If the beam is smaller than the target, then we need only set A equal to the area covered by the beam. Then $FA \to n_{\text{inc}}$, the total number of incident particles per unit time. In both cases, now, if we divide (2.4) by FA, we have the probability for the scattering of a *single* particle in a thickness δx,

$$\text{Prob. of interaction in } \delta x = N\sigma\,\delta x. \tag{2.5}$$

This is an important quantity and we will come back to this probability later.

2.1.2 Interaction Probability in a Distance x. Mean Free Path

In the previous section, we discussed the probability for the interaction of a particle traveling through a thin slab of matter containing many interaction centers. Let us consider the more general case of *any* thickness x. To do this, we ask the opposite question: what is the probability for a particle *not* to suffer an interaction in a distance x? This is known as the *survival* probability and may be calculated in the following way. Let

$P(x)$: probability of *not* having an interaction after a distance x,
$w\,dx$: probability of having an interaction between x and $x+dx$.

The probability of *not* having an interaction between x and $x+dx$ is then

$$\begin{aligned} &P(x+dx) = P(x)(1-w\,dx), \\ &P(x)+\frac{dP}{dx}dx = P - Pw\,dx, \\ &dP = -wP\,dx, \\ &P = C\exp(-w), \end{aligned} \tag{2.6}$$

where C is a constant. Requiring that $P(0) = 1$, we find $C = 1$. The probability of the particle surviving a distance x is thus exponential in distance. From this, of course, we see immediately that the probability of suffering an interaction *anywhere* in the distance x is just

$$P_{\text{int}}(x) = 1 - \exp(-wx)\,, \tag{2.7}$$

while the probability of the particle suffering a collision between x and $x+dx$ after surviving the distance x is

$$P(x)dx = \exp(-wx)\, w\, dx\,. \tag{2.8}$$

Now let us calculate the mean distance, λ, traveled by the particle without suffering a collision. This is known as the *mean free path*. Thus,

$$\lambda = \frac{\int xP(x)\,dx}{\int P(x)\,dx} = \frac{1}{w}\,. \tag{2.9}$$

Intuitively, λ must be related to the density of interaction centers and the cross-section, for as we have seen, this governs the probability of interaction. To find this relation, let us return to our slab of material. For a small thickness δx, the interaction probability (2.7) can then be approximated as

$$P_{\text{int}} = 1 - \left(1 - \frac{\delta x}{\lambda} + \ldots\right) \simeq \frac{\delta x}{\lambda}\,, \tag{2.10}$$

where we have expanded the exponential. Comparing with (2.5), we thus find,

$$\lambda = 1/N\sigma\,, \tag{2.11}$$

so that our survival probability becomes

$$P(x) = \exp\left(\frac{-x}{\lambda}\right) = \exp(-N\sigma x)\,, \tag{2.12}$$

and the interaction probabilities

$$P_{\text{int}}(x) = 1 - \exp\left(\frac{-x}{\lambda}\right) = 1 - \exp(-N\sigma x)\,, \tag{2.13}$$

$$F(x)\,dx = \exp\left(\frac{-x}{\lambda}\right)\frac{dx}{\lambda} = \exp(-N\sigma x)\, N\sigma\, dx\,. \tag{2.14}$$

2.1.3 Surface Density Units

A unit very often used for expressing thicknesses of absorbers is the *surface density* or *mass thickness*. This is given by the mass density of the material times its thickness in normal units of length, i.e.,

$$\text{mass thickness} \triangleq \rho \cdot t \tag{2.15}$$

with ρ: mass density, t: thickness, which, of course, yields dimensions of mass per area, e.g. g/cm^2.

For discussing the interaction of radiation in matter, mass thickness units are more convenient than normal length units because they are more closely related to the density

of interaction centers. They thus have the effect of normalizing materials of differing mass densities. As will be seen later, equal mass thicknesses of different materials will have roughly the same effect on the same radiation.

2.2 Energy Loss of Heavy Charged Particles by Atomic Collisions

In general, two principal features characterize the passage of charged particles through matter: (1) a loss of energy by the particle and (2) a deflection of the particle from its incident direction. These effects are primarily the result of two processes:

1) inelastic collisions with the atomic electrons of the material
2) elastic scattering from nuclei.

These reactions occur many times per unit path length in matter and it is their cumulative result which accounts for the two principal effects observed. These, however, are by no means the only reactions which can occur. Other processes include

3) emission of Cherenkov radiation
4) nuclear reactions
5) bremsstrahlung.

In comparison to the atomic collision processes, they are extremely rare, however, and with the exception of Cherenkov radiation, will be ignored in this treatment.

For reasons which will become clearer in the following sections, it is necessary to separate charged particles into two classes: (1) electrons and positrons, and (2) heavy particles, i.e., particles heavier than the electron. This latter group includes the muons, pions, protons, α-particles and other light nuclei. Particles heavier than this, i.e., the heavy ions, although technically part of this latter group, are excluded in this discussion because of additional effects which arise.

Of the two electromagnetic processes, the inelastic collisions are almost solely responsible for the energy loss of heavy particles in matter. In these collisions ($\sigma \approx 10^{-17} - 10^{-16}\,\mathrm{cm}^2$!), energy is transferred from the particle to the atom causing an ionization or excitation of the latter. The amount transferred in each collision is generally a very small fraction of the particle's total kinetic energy; however, in normally dense matter, the number of collisions per unit path length is so large, that a substantial cumulative enery loss is observed even in relatively thin layers of material. A 10 MeV proton, for example, already loses *all* of its energy in only 0.25 mm of copper! These atomic collisions are customarily divided into two groups: *soft* collisions in which only an excitation results, and *hard* collisions in which the energy transferred is sufficient to cause ionization. In some of the *hard* reactions, enough energy is, in fact, transferred such that the electron itself causes substantial secondary ionization. These high-energy recoil electrons are sometimes referred to as *δ-rays* or *knock-on* electrons.

Elastic scattering from nuclei also occurs frequently although not as often as electron collisions. In general very little energy is transferred in these collisions since the masses of the nuclei of most materials are usually large compared to the incident particle. In cases where this is not true, for example, an α-particle in hydrogen, some energy is also lost through this mechanism. Nevertheless, the major part of the energy loss is still due to atomic electron collisions.

The inelastic collisions are, of course, statistical in nature, occurring with a certain quantum mechanical probability. However, because their number per macroscopic pathlength is generally large, the fluctuations in the total energy loss are small and one can meaningfully work with the average energy loss per unit path length. This quantity, often called the *stopping power* or simply dE/dx, was first calculated by Bohr using classical arguments and later by Bethe, Bloch and others using quantum mechanics. Bohr's calculation is, nevertheless, very instructive and we will briefly present a simplified version due to *Jackson* [2.1] here.

2.2.1 Bohr's Calculation – The Classical Case

Consider a heavy particle with a charge ze, mass M and velocity v passing through some material medium and suppose that there is an atomic electron at some distance b from the particle trajectory (see Fig. 2.2). We assume that the electron is free and initially at rest, and furthermore, that it only moves very slightly during the interaction with the heavy particle so that the electric field acting on the electron may be taken at its initial position. Moreover, after the collision, we assume the incident particle to be essentially undeviated from its original path because of its much larger mass ($M \gg m_e$). This is one reason for separating electrons from heavy particles!

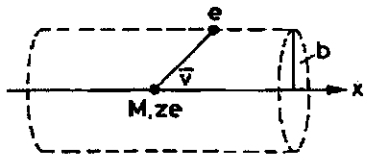

Fig. 2.2. Collision of a heavy charged particle with an atomic electron

Let us now try to calculate the energy gained by the electron by finding the momentum impulse it receives from colliding with the heavy particle. Thus

$$I = \int F\,dt = e\int E_\perp\,dt = e\int E_\perp \frac{dt}{dx}\,dx = e\int E_\perp \frac{dx}{v}, \tag{2.16}$$

where only the component of the electric field $E_\perp$ perpendicular to the particle trajectory enters because of symmetry. To calculate the integral $\int E_\perp\,dx$, we use Gauss' Law over an infinitely long cylinder centered on the particle trajectory and passing through the position of the electron. Then

$$\int E_\perp 2\pi b\,dx = 4\pi ze\,, \quad \int E_\perp\,dx = \frac{2ze}{b}\,, \tag{2.17}$$

so that

$$I = \frac{2ze^2}{bv} \tag{2.18}$$

and the energy gained by the electron is

$$\Delta E(b) = \frac{I^2}{2m_e} = \frac{2z^2e^4}{m_e v^2 b^2}\,. \tag{2.19}$$

If we let N_e be the density of electrons, then the energy lost to all the electrons located at a distance between b and $b+db$ in a thickness dx is

$$-dE(b) = \Delta E(b)\, N_e\, dV = \frac{4\pi z^2 e^4}{m_e v^2} N_e \frac{db}{b} dx\,, \tag{2.20}$$

where the volume element $dV = 2\pi b\, db\, dx$. Continuing in a straight forward manner, one would at this point be tempted to integrate (2.20) from $b = 0$ to ∞ to get the total energy loss; however, this is contrary to our original assumptions. For example, collisions at very large b would not take place over a short period of time, so that our impulse calculation would not be valid. As well, for $b = 0$, we see that (2.19) gives an infinite energy transfer, so that (2.19) is not valid at small b either. Our integration, therefore, must be made over some limits $b_{\min}$ and $b_{\max}$ between which (2.19) holds. Thus,

$$-\frac{dE}{dx} = \frac{4\pi z^2 e^4}{m_e v^2} N_e \ln \frac{b_{\max}}{b_{\min}}\,. \tag{2.21}$$

To estimate values for $b_{\min}$ and $b_{\max}$, we must make some physical arguments. Classically, the maximum energy transferable is in a head-on collision where the electron obtains an energy of $\frac{1}{2} m_e (2v)^2$. If we take relativity into account, this becomes $2\gamma^2 m_e v^2$, where $\gamma = (1-\beta^2)^{-1/2}$ and $\beta = v/c$. Using (2.19) then, we find

$$\frac{2z^2 e^4}{m_e v^2 b_{\min}^2} = 2\gamma^2 m v^2, \qquad b_{\min} = \frac{ze^2}{\gamma m_e v^2}\,. \tag{2.22}$$

For $b_{\max}$, we must recall now that the electrons are not free but bound to atoms with some orbital frequency ν. In order for the electron to absorb energy, then, the perturbation caused by the passing particle must take place in a time short compared to the period $\tau = 1/\nu$ of the bound electron, otherwise, the perturbation is adiabatic and no energy is transferred. This is the principle of *adiabatic invariance*. For our collisions the typical interaction time is $t \approx b/v$, which relativistically becomes $t \Rightarrow t/\gamma = b/(\gamma v)$, so that

$$\frac{b}{\gamma v} \leq \tau = \frac{1}{\bar{\nu}}\,. \tag{2.23}$$

Since there are several bound electron states with different frequencies ν, we have used here a mean frequency, $\bar{\nu}$, averaged over all bound states. An upper limit for b, then, is

$$b_{\max} = \frac{\gamma v}{\bar{\nu}}\,. \tag{2.24}$$

Substituting into (2.21), we find

$$-\frac{dE}{dx} = \frac{4\pi z^2 e^4}{m_e v^2} N_e \ln \frac{\gamma^2 m v^3}{z e^2 \bar{\nu}}\,. \tag{2.25}$$

This is essentially Bohr's classical formula. It gives a reasonable description of the energy loss for very heavy particles such as the α-particle or heavier nuclei. However,

for lighter particles, e.g. the proton, the formula breaks down because of quantum effects. It nevertheless contains all the essential features of electronic collision loss by charged particles.

2.2.2 The Bethe-Bloch Formula

The correct quantum-mechanical calculation was first performed by Bethe, Bloch and other authors. In the calculation the energy transfer is parametrized in terms of momentum transfer rather than the impact parameter. This, of course, is more realistic since the momentum transfer is a measurable quantity whereas the impact parameter is not. The formula obtained is then

$$-\frac{dE}{dx} = 2\pi N_a r_e^2 m_e c^2 \rho \frac{Z}{A}\frac{z^2}{\beta^2}\left[\ln\left(\frac{2m_e\gamma^2 v^2 W_{max}}{I^2}\right) - 2\beta^2\right]. \tag{2.26}$$

Equation (2.26) is commonly known as the *Bethe-Bloch formula* and is the basic expression used for energy loss calculations. In practice, however, two corrections are normally added: the *density effect* correction δ, and the *shell* correction C, so that

$$-\frac{dE}{dx} = 2\pi N_a r_e^2 m_e c^2 \rho \frac{Z}{A}\frac{z^2}{\beta^2}\left[\ln\left(\frac{2m_e\gamma^2 v^2 W_{max}}{I^2}\right) - 2\beta^2 - \delta - 2\frac{C}{Z}\right], \tag{2.27}$$

with

$$2\pi N_a r_e^2 m_e c^2 = 0.1535\ \text{MeVcm}^2/\text{g}$$

r_e: classical electron radius $= 2.817 \times 10^{-13}$ cm
m_e: electron mass
N_a: Avogadro's number $= 6.022 \times 10^{23}\ \text{mol}^{-1}$
I: mean excitation potential
Z: atomic number of absorbing material
A: atomic weight of absorbing material
ρ: density of absorbing material
z: charge of incident particle in units of e
$\beta = v/c$ of the incident particle
$\gamma = 1/\sqrt{1-\beta^2}$
δ: density correction
C: shell correction
W_{max}: maximum energy transfer in a single collision.

The maximum energy transfer is that produced by a head-on or *knock-on* collision. For an incident particle of mass M, kinematics gives

$$W_{max} = \frac{2m_e c^2 \eta^2}{1 + 2s\sqrt{1+\eta^2} + s^2}, \tag{2.28}$$

where $s = m_e/M$ and $\eta = \beta\gamma$. Moreover, if $M \gg m_e$, then

$$W_{max} \simeq 2m_e c^2 \eta^2 .$$

The Mean Excitation Potential. The mean excitation potential, I, is the main parameter of the Bethe-Bloch formula and is essentially the average orbital frequency $\bar{\nu}$ from Bohr's formula times Planck's constant, $h\bar{\nu}$. It is theoretically a logarithmic average of

ν weighted by the so-called oscillator strengths of the atomic levels. In practice, this is a very difficult quantity to calculate since the oscillator strengths are unknown for most materials. Instead, values of I for several materials have been deduced from actual measurements of dE/dx and a semi-empirical formula for I vs Z fitted to the points. One such formula is

$$\begin{aligned} \frac{I}{Z} &= 12+\frac{7}{Z}\,\text{eV} && Z<13 \\ \frac{I}{Z} &= 9.76+58.8Z^{-1.19}\,\text{eV} && Z\geq 13\,. \end{aligned} \tag{2.29}$$

It has been shown, however, that I actually varies with Z in a more complicated manner [2.2]. In particular, there are local irregularities or *wiggles* due to the closing of certain atomic shells. Improved values of I are given in Table 2.1 for several materials. A more extensive list may be found in the articles by *Sternheimer* et al. [2.2–3].

The Shell and Density Corrections. The quantities δ and C are corrections to the Bethe-Bloch formula which are important at high and low energies respectively.

The *density effect* arises from the fact that the electric field of the particle also tends to polarize the atoms along its path. Because of this polarization, electrons far from the path of the particle will be shielded from the full electric field intensity. Collisions with these outer lying electrons will therefore contribute less to the total energy loss than predicted by the Bethe-Bloch formula. This effect becomes more important as the particle energy increases, as can be seen from the expression for b_{max} in (2.24). Clearly as the velocity increases, the radius of the cylinder over which our integration is performed also increases, so that distant collisions contribute more and more to the total energy loss. Moreover, it is clear that this effect depends on the density of the material (hence the term *"density"* effect), since the induced polarization will be greater in condensed materials than in lighter substances such as gases. A comparison of the Bethe-Bloch formula with and without corrections is shown in Fig. 2.3.

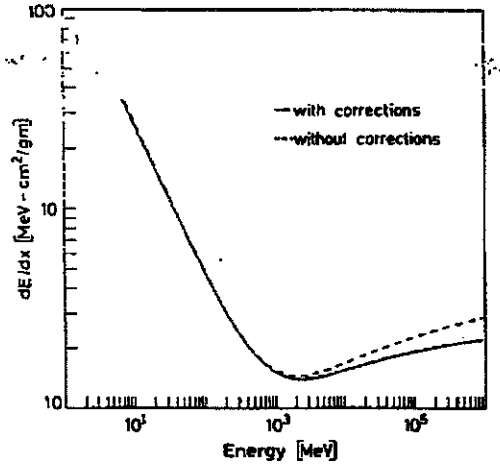

Fig. 2.3. Comparison of the Bethe-Bloch formula with and without the shell and density corrections. The calculation shown here is for copper

Values for δ are given by a formula due to Sternheimer:

$$\delta = \begin{cases} 0 & X < X_0 \\ 4.6052X + C + a(X_1 - X)^m & X_0 < X < X_1 \\ 4.6052X + C & X > X_1, \end{cases} \quad (2.3($$

where $X = \log_{10}(\beta\gamma)$.

The quantities X_0, X_1, C, a and m depend on the absorbing material. The paran eter C is defined as

$$C = -\left(2\ln\frac{I}{h\nu_p} + 1\right), \quad (2.31$$

where $h\nu_p$ is the so-called plasma frequency of the material, i.e.,

$$\nu_p = \sqrt{\frac{N_e e^2}{\pi m_e}}, \quad (2.3$$

where N_e (density of electrons) $= N_a \rho Z/A$. The remaining constants are determined b fitting (2.30) to experimental data. Values for several materials are presented in Tabl 2.1. A more complete listing may be found in *Sternheimer* et al. [2.3].

The *shell* correction accounts for effects which arise when the velocity of the ir cident particle is comparable or smaller than the orbital velocity of the bound electron At such energies, the assumption that the electron is stationary with respect to th incident particle is no longer valid and the Bethe-Bloch formula breaks down. Th correction is generally small as can be seen in Fig. 2.3. We give there an empiric formula [2.4] for this correction, valid for $\eta \geq 0.1$:

$$C(I,\eta) = (0.422377\,\eta^{-2} + 0.0304043\,\eta^{-4} - 0.00038106\,\eta^{-6}) \times 10^{-6} I^2 + (3.850190\,\eta^{-2} - 0.1667989\,\eta^{-4} + 0.00157955\,\pi^{-6}) \times 10^{-9} I^3, \quad (2.3$$

where $\eta = \beta\gamma$ and I is the mean excitation potential in eV.

Table 2.1. Constants for the density effect correction

Material	I [eV]	$-C$	a	m	X_1	X_0
Graphite density = 2	78	2.99	0.2024	3.00	2.486	−0.0351
Mg	156	4.53	0.0816	3.62	3.07	0.1499
Cu	322	4.42	0.1434	2.90	3.28	0.0254
Al	166	4.24	0.0802	3.63	3.01	0.1708
Fe	286	4.29	0.1468	2.96	3.15	−0.0012
Au	790	5.57	0.0976	3.11	3.70	0.2021
Pb	823	6.20	0.0936	3.16	3.81	0.3776
Si	173	4.44	0.1492	3.25	2.87	0.2014
NaI	452	6.06	0.1252	3.04	3.59	0.1203
N_2	82	10.5	0.1534	3.21	4.13	1.738
O_2	95	10.7	0.1178	3.29	4.32	1.754
H_2O	75	3.50	0.0911	3.48	2.80	0.2400
lucite	74	3.30	0.1143	3.38	2.67	0.1824
Air	85.7	10.6	0.1091	3.40	4.28	1.742
BGO	534	5.74	0.0957	3.08	3.78	0.0456
Plastic Scint.	64.7	3.20	0.1610	3.24	2.49	0.1464

Other Corrections. In addition to the shell and density effects, the validity and accuracy of the Bethe-Bloch formula may be extended by including a number of other corrections pertaining to radiation effects at ultrarelativistic velocities, kinematic effects due to the assumption of an infinite mass for the projectile, higher-order QED processes, higher-order terms in the scattering cross-section, corrections for the internal structure of the particle, spin effects and electron capture at very slow velocities. With the exception of electron-capture effects with heavy ions, these are usually negligible to within $\approx 1\%$. An outline of these additional factors may be found in the articles by *Ahlen* [2.5–6]. For *"elementary"* particles, the Bethe-Bloch formula with the shell and density corrections is more than sufficient however.

2.2.3 Energy Dependence

An example of the energy dependence of dE/dx is shown in Fig. 2.4 which plots the Bethe-Bloch formula as a function of kinetic energy for several different particles. At non-relativistic energies, dE/dx is dominated by the overall $1/\beta^2$ factor and decreases with increasing velocity until about $v \approx 0.96\,c$, where a minimum is reached. Particles at this point are known as *minimum ionizing*. Note that the minimum value of dE/dx is almost the same for all particles of the same charge. As the energy increases beyond this point, the term $1/\beta^2$ becomes almost constant and dE/dx rises again due to the logarithmic dependence of (2.27). This *relativistic rise* is cancelled, however, by the density correction as seen in Fig. 2.3.

For energies below the minimum ionizing value, each particle exhibits a dE/dx curve which, in most cases, is distinct from the other particle types. This characteristic is often exploited in particle physics as a means for identifying particles in this energy range.

Not shown in Fig. 2.4, is the very low energy region, where the Bethe-Bloch formula breaks down. At low velocities comparable to the velocity of the orbital electrons of the material, dE/dx, in fact, reaches a maximum and then drops sharply again. Here, a number of complicated effects come into play. The most important of these is the tendency of the particle to pick up electrons for part of the time. This lowers the effective charge of the particle and thus its stopping power. Calculating this effective charge can be a difficult problem especially for heavy ions.

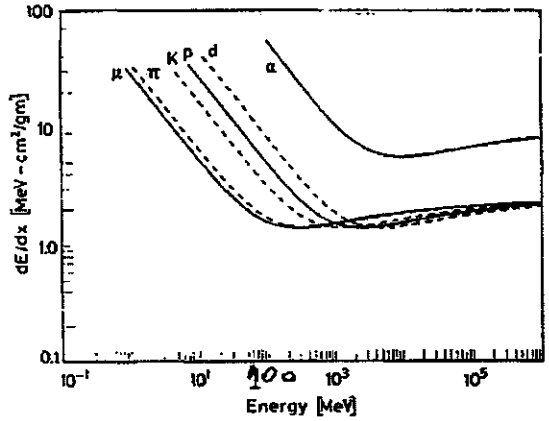

Fig. 2.4. The stopping power dE/dx as function of energy for different particles

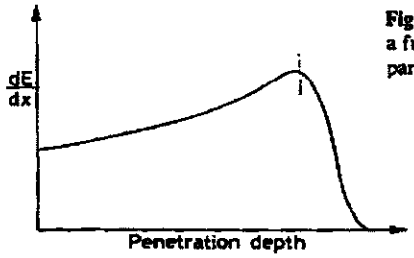

Fig. 2.5. A typical Bragg curve showing the variation of dE/dx as a function of the penetration depth of the particle in matter. The particle is more ionizing towards the end of its path

From Fig. 2.4, it is clear that as a heavy particle slows down in matter, its rate of energy loss will change as its kinetic energy changes. And indeed, more energy per unit length will be deposited towards the end of its path rather than at its beginning. This effect is seen in Fig. 2.5 which shows the amount of ionization created by a heavy particle as a function of its position along it slowing-down path. This is known as a *Bragg* curve, and, as can be seen, most of the energy is deposited near the end of the trajectory. At the very end, however, it begins to pick up electrons and the dE/dx drops. This behavior is particularly used in medical applications of radiation where it is desired to deliver a high dose of radiation to deeply embedded malignant growths with a minimum of destruction to the overlaying tissue.

2.2.4 Scaling Laws for dE/dx

For particles in the same material medium, the Bethe-Bloch formula can be seen to be of the form

$$-\frac{dE}{dx} = z^2 f(\beta)\,, \tag{2.34}$$

where $f(\beta)$ is a function of the particle velocity only. Thus, the energy loss in any given material is dependent only on the charge and velocity of the particle. Since the kinetic energy $T = (\gamma - 1)Mc^2$, the velocity is a function of T/M, so that $\beta = g(T/M)$. We can therefore transform (2.34) to

$$-\frac{dE}{dx} = z^2 f'\left(\frac{T}{M}\right). \tag{2.35}$$

This immediately suggests a scaling law: if we know the dE/dx for a particle of mass M_1 and charge z_1, then the energy loss of a particle of mass M_2, charge z_2 and energy T_2 in the same material may be found from the values of particle 1 by scaling the energy of particle 2 to $T = T_2(M_1/M_2)$ and multiplying by the charge ratio $(z_2/z_1)^2$, i.e.,

$$-\frac{dE_2}{dx}(T_2) = -\frac{z_2^2}{z_1^2}\frac{dE_1}{dx}\left(T_2\frac{M_1}{M_2}\right). \tag{2.36}$$

2.2.5 Mass Stopping Power

When dE/dx is expressed in units of mass thickness, it is found to vary little over a wide range of materials. Indeed, if we make the dependence on material type more evident in the Bethe-Bloch formula, we find

$$-\frac{dE}{d\varepsilon} = -\frac{1}{\rho}\frac{dE}{dx} = z^2 \frac{Z}{A} f(\beta, I), \tag{2.37}$$

where $d\varepsilon = \rho\, dx$. For not too different Z, the ratio (Z/A), in fact, varies little. This is also true of the dependence on $I(Z)$ since it appears in a logarithm. $dE/d\varepsilon$, therefore, is almost independent of material type. A 10 MeV proton, for example, will lose about the same amount of energy in 1 g/cm^2 of copper as it will in 1 g/cm^2 of aluminium or iron, etc. As will also be seen, these units are also more convenient when dE/dx's are combined for mixed materials.

2.2.6 dE/dx for Mixtures and Compounds

The dE/dx formula which we have given so far applies to pure elements. What about dE/dx for compounds and mixtures? Here, if accurate values are desired, one must usually resort to direct measurements; however, a good approximate value can be found in most cases by averaging dE/dx over each element in the compound weighted by the fraction of electrons belonging to each element (*Bragg's Rule*). Thus

$$\frac{1}{\rho}\frac{dE}{dx} = \frac{w_1}{\rho_1}\left(\frac{dE}{dx}\right)_1 + \frac{w_2}{\rho_2}\left(\frac{dE}{dx}\right)_2 + \ldots, \tag{2.38}$$

where w_1, w_2, etc. are the fractions by *weight* of elements 1, 2, ... in the compound. More explicitly, if a_i is the number of atoms of the ith element in the molecule M, then

$$w_i = \frac{a_i A_i}{A_m}, \tag{2.39}$$

where A_i is the atomic weight of ith element, $A_m = \sum a_i A_i$.

By expanding (2.38) explicitly and regrouping terms, we can define effective values for Z, A, I, etc. which may be used directly in (2.27),

$$Z_{\text{eff}} = \sum a_i Z_i, \tag{2.40}$$

$$A_{\text{eff}} = \sum a_i A_i, \tag{2.41}$$

$$\ln I_{\text{eff}} = \sum \frac{a_i Z_i \ln I_i}{Z_{\text{eff}}}, \tag{2.42}$$

$$\delta_{\text{eff}} = \sum \frac{a_i Z_i \delta_i}{Z_{\text{eff}}}, \tag{2.43}$$

$$C_{\text{eff}} = \sum a_i C_i. \tag{2.44}$$

Note here the convenience of working with the mass stopping power, $1/\rho(dE/dx)$, rather than the linear stopping power dE/dx.

2.2.7 Limitations of the Bethe-Bloch Formula and Other Effects

The Bethe-Bloch formula as given in (2.27) with the shell and density effect corrections is the usual expression employed in most dE/dx calculations. For *elementary* particles

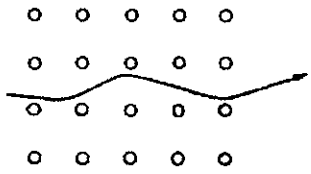

Fig. 2.6. Schematic diagram of channeling in crystalline materials. The particle suffers a series of correlated scatterings which guides it down an open channel of the lattice

and nuclei up to the α-particle, this formula generally gives results accurate to within a few percent for velocities ranging from the relativistic region down to $\beta \simeq 0.1$. This accuracy may be increased and extended to higher-Z nuclei up to $Z \simeq 26$ by including the charge-dependent corrections mentioned earlier [2.5–6].

For $\beta \leq 0.05$, many of the assumptions inherent in the Bethe-Bloch formula are no longer valid even with the corrections. Between $0.01 < \beta < 0.05$, in fact, there is still no satisfactory theory for protons. For heavier nuclei, this is even more the case because of electron capture effects. Some empirical formulae for this energy range may be found in [2.7]. Below $\beta = 0.01$, however, a successful explanation of energy loss is given by the theory of *Lindhard* [2.8].

2.2.8 Channeling

An important exception to the applicability of the Bethe-Bloch formula is in the case of *channeling* in materials having a spatially symmetric atomic structure, i.e., crystals. This is an effect which occurs only when the particle is incident at angles less than some critical angle with respect to a symmetry axis of the crystal. As it passes through the crystal planes, the particle, in fact, suffers a series of correlated small-angle scatterings which guide it down an open crystal channel. Figure 2.6 illustrates this schematically. As can be seen, the correlated scatterings cause the particle to follow a slowly oscillating trajectory which keeps it within the open channel over relatively long distances. The wavelength of the trajectory is generally many lattice lengths long. The net effect of this, of course, is that the particle encounters less electrons than it normally would in an amorphous material (which is assumed by the Bethe-Bloch calculation). When the particle undergoes channeling, therefore, its rate of energy loss is greatly reduced. When working with crystalline materials, it is important therefore to be aware of the crystal orientation with respect to the incident particles so as to avoid (or achieve, if that is the case) channeling effects.

In general, the critical angle necessary for channeling is small ($\simeq 1°$ for $\beta \simeq 0.1$) and decreases with energy. It can be estimated by the formula [2.5]

$$\phi_c \simeq \frac{\sqrt{z Z a_0 A d}}{1670 \beta \sqrt{\gamma}}, \tag{2.45}$$

where a_0 is the Bohr radius, and d the interatomic spacing. For $\phi > \phi_c$, channeling does not occur and the material may be treated as amorphous. A more detailed discussion of channeling and the stopping power under such conditions can be found in the review by *Gemmell* [2.8].

2.2.9 Range

Knowing that charged particles lose their energy in matter, a natural question to ask is: How far will the particles penetrate before they lose all of their energy? Moreover, if we assume that the energy loss is continuous, this distance must be a well defined number, the same for all identical particles with the same initial energy in the same type of material. This quantity is called the *range* of the particle, and depends on the type of material, the particle type and its energy.

Experimentally, the range can be determined by passing a beam of particles at the desired energy through different thicknesses of the material in question and measuring

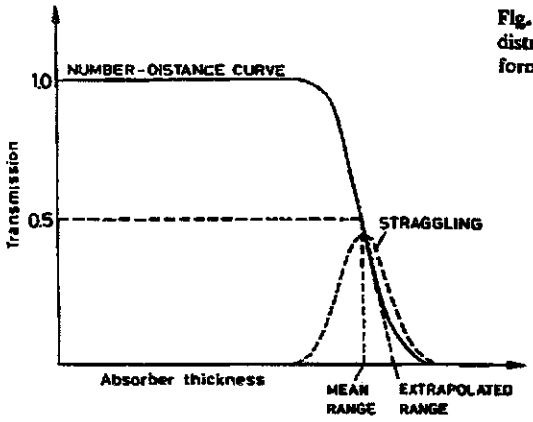

Fig. 2.7. Typical range number-distance curve. The distribution of ranges is approximately Gaussian in form

the ratio of transmitted to incident particles. A typical curve of this ratio versus absorber thickness, known as a *range number-distance* curve, is shown in Fig. 2.7. As can be seen, for small thicknesses, all (or practically all) the particles manage to pass through. As the range is approached this ratio drops. The surprising thing, however, is that the ratio does not drop immediately to the background level, as expected of a well defined quantity. Instead the curve slopes down over a certain spread of thicknesses. This result is due to the fact that the energy loss is *not* in fact continuous, but statistical in nature. Indeed, two identical particles with the same initial energy will *not* in general suffer the same number of collisions and hence the same energy loss. A measurement with an ensemble of identical particles, therefore, will show a statistical distribution of ranges centered about some mean value. This phenomenon is known as *range straggling*. In a first approximation, this distribution is gaussian in form. The mean value of the distribution is known as the *mean range* and corresponds to the midpoint on the descending slope of Fig. 2.7. This is the thickness at which roughly half the particles are absorbed. More commonly, however, what is desired is the thickness at which all the particles are absorbed, in which case the point at which the curve drops to the background level should be taken. This point is usually found by taking the tangent to the curve at the midpoint and extrapolating to the zero-level. This value is known as the *extrapolated* or *practical range* (see Fig. 2.7).

From a theoretical point of view, we might be tempted to calculate the mean range of a particle of a given energy, T_0, by integrating the dE/dx formula,

$$S(T_0) = \int_0^{T_0} \left(\frac{dE}{dx}\right)^{-1} dE\,. \tag{2.46}$$

This yields the approximate pathlength travelled. Equation (2.46) ignores the effect of multiple Coulomb scattering, however, which causes the particle to follow a zigzag path through the absorber (see Fig. 2.14). Thus, the range, defined as the straight-line thickness, will generally be smaller than the total zigzag pathlength.

As it turns out, however, the effect of multiple scattering is generally small for heavy charged particles, so that the total path length is, in fact, a relatively good approximation to the straight-line range. In practice, a semi-empirical formula must be used,

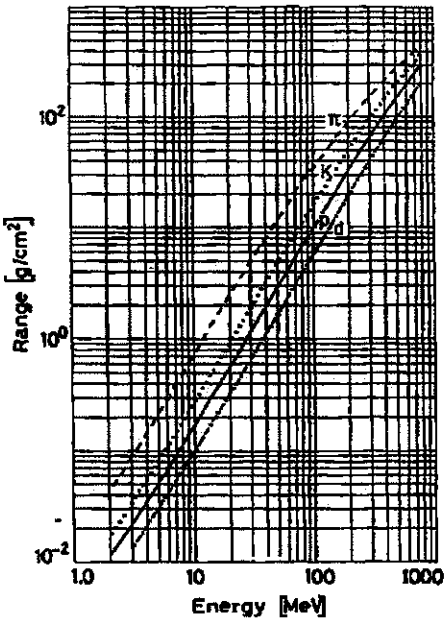

Fig. 2.8. Calculated range curves of different heavy particles in aluminium

$$R(T_0) = R_0(T_{\min}) + \int_{T_{\min}}^{T_0} \left(\frac{dE}{dx}\right)^{-1} dE\,, \tag{2.47}$$

where $T_{\min}$ is the minimum energy at which the dE/dx formula is valid, and $R_0(T_{\min})$ is an empirically determined constant which accounts for the remaining low energy behavior of the energy loss. Results accurate to within a few percent can be obtained in this manner.[2] Figure 2.8 shows some typical range-energy curves for different particles calculated by a numerical integration of the Bethe-Bloch formula. From its almost linear form on the log-log scale, one might expect a relation of the type

$$R \propto E^b\,. \tag{2.48}$$

This can also be seen from the stopping power formula, which at not too high energies, is dominated by the β^{-2} term,

$$-dE/dx \propto \beta^{-2} \propto T^{-1}\,, \tag{2.49}$$

where T is the kinetic energy. Integrating, we thus find

$$R \propto T^2\,, \tag{2.50}$$

[2] We might emphasize here that the range as calculated by (2.47) only takes into account energy losses due to atomic collisions and is valid only as long as atomic collisions remain the principal means of energy loss. At very high energies, where the range becomes larger than the mean free path for a nuclear interaction or for bremsstrahlung emission, this is no longer true and one must take into account these latter interactions as well.

which is consistent with our rough guess. A more accurate fit in this energy range, in fact, gives

$$R \propto T^{1.75}, \tag{2.51}$$

which is not too far from our simple calculation. This is only one of many theoretical and semi-empirical formulas which cover many energy ranges and materials. A discussion of some of these relations is given in the article by *Bethe* and *Ashkin* [2.10].

Range-energy relations of this type are extremely useful as they provide an accurate means of measuring the energy of the particles. This was one of the earliest uses of range measurements. As we will see later, they are also necessary for deciding the sizes of detectors to be used in an experiment or in determining the thickness of radiation shielding, among other things.

Because of the scaling of dE/dx, a scaling law for ranges may also be derived. Using (2.36), it is easy then to see

$$R_2(T_2) = \frac{M_2}{M_1}\frac{z_1^2}{z_2^2} R_1\left(T_2 \frac{M_1}{M_2}\right) \tag{2.52}$$

for different particles in the same medium.

For the same particle in different materials, a rough relation known as the *Bragg-Kleeman* rule also exists

$$\frac{R_1}{R_2} = \frac{\rho_2}{\rho_1}\frac{\sqrt{A_1}}{\sqrt{A_2}}, \tag{2.53}$$

where ρ and A are the densities and atomic numbers of the materials. For compounds, a rough approximation for the range can also be found from the formula

$$R_{\text{comp}} = \frac{A_{\text{comp}}}{\sum \frac{a_i A_i}{R_i}}, \tag{2.54}$$

where A_{comp} is the molecular weight of the compound, A_i and R_i are the atomic weight and range of the ith constituent element, respectively, and a_i is the number of atoms of the ith element in the compound molecule.

2.3 Cherenkov Radiation

Cherenkov radiation arises when a charged particle in a material medium moves faster than the speed of light in that same medium. This speed is given by

$$\beta c = v = c/n, \tag{2.55}$$

where n is the index of refraction and c is the speed of light in a vacuum. A particle emitting Cherenkov radiation must therefore have a velocity

$$v_{\text{part}} > c/n. \tag{2.56}$$